

# REPORT DOCUMENTATION PAGE

Public reporting burden for this collection of information is estimated to average 1 hour per response, including the time for reviewing instructions, searching existing data sources, gathering the required data, completing and reviewing this collection of information. Send comments regarding this burden estimate or any other aspect of this burden to Department of Defense, Washington Headquarters Services, Directorate for Information Operations and Reports (0704-018 4302). Respondents should be aware that notwithstanding any other provision of law, no person shall be subject to any penalty for failing to provide information if it does not have an OMB control number. PLEASE DO NOT RETURN YOUR FORM TO THE ABOVE ADDRESS.

AFRL-SR-AR-TR-02-

0231

**1. REPORT DATE (DD-MM-YYYY)**

06/21/02

**2. REPORT TYPE**

Final

**3. DATES COVERED (from - to)**

6/1/98-11/30/01

**4. TITLE AND SUBTITLE**

"Self-Assembled Monolayers at the Lithium Electrode/Polymer

Electrolyte Interface"

**5a. CONTRACT NUMBER**

**5b. GRANT NUMBER**

F49620-98-1-0435

**5c. PROGRAM ELEMENT NUMBER**

61103D

**5d. PROJECT NUMBER**

3484

**5e. TASK NUMBER**

BS

**5f. WORK UNIT NUMBER**

**6. AUTHOR(S)**

Dale Teeters, Professor of Chemistry

Department of Chemistry and Biochemistry

**7. PERFORMING ORGANIZATION NAME(S) AND ADDRESS(ES)**

The University of Tulsa

600 South College Avenue

Tulsa, OK 74104-3189

**8. PERFORMING ORGANIZATION REPORT NUMBER**

4

**9. SPONSORING / MONITORING AGENCY NAME(S) AND ADDRESS(ES)**

AFOSR/LN

110 Duncan Avenue, Room B115

Bolling AFB, DC 20332-8050

**10. SPONSOR/MONITOR'S ACRONYM(S)**

**11. SPONSOR/MONITOR'S REPORT NUMBER(S)**

**12. DISTRIBUTION / AVAILABILITY STATEMENT**

Approved for Public Release; Distribution is Unlimited

**13. SUPPLEMENTARY NOTES**

**14. ABSTRACT**

The proposed work involved the placement of self-assembled monolayers (SAMs) on the polymer electrolyte surface to deter and/or stabilize the formation of the passivation layer between the polymer electrolyte and the lithium electrode. This work combines two very scientifically and technologically important areas, lithium polymer batteries and self-assembled monolayers, resulting in a novel study that has advanced the basic understanding of the electrode/electrolyte interface and the development of better battery systems.

20020816 065

**15. SUBJECT TERMS**

Self-Assembled Monolayers at the Lithium Electrode/Polymer Electrolyte Interface

**16. SECURITY CLASSIFICATION OF:**

none

**17. LIMITATION OF ABSTRACT**

**18. NUMBER OF PAGES**

74

**19a. NAME OF RESPONSIBLE PERSON**

Dale Teeters

**19b. TELEPHONE NUMBER (include area code)**

(918) 631-3147

**a. REPORT**

**b. ABSTRACT**

**c. THIS PAGE**

**Self-Assembled Monolayers at the Lithium Electrode/Polymer  
Electrolyte Interface**

**Final Report  
Air Force Office of Scientific Research  
Grant No. F49620-98-1-0435**

June 21, 2002

Dale Teeters, Professor of Chemistry  
Department of Chemistry and Biochemistry  
The University of Tulsa  
600 S. College Ave.  
Tulsa, OK 74104

## Table of Contents

I.	Objectives .....	3
II.	Executive Summary of Work.....	3
III.	Significance of Work .....	6
IV.	Technical Issues to be Addressed in the Future .....	6
V.	Description of Research	
	Chapter 1. Placement and Characterization of Self-Assembled Monolayers at the Electrode/Electrolyte Interface and the Ability of the Monolayer to Prevent Passivation.....	8
	Chapter 2. Chemistry of the Polymer Electrolyte/Lithium Metal Interface, With and Without Self-Assembled Monolayer Protection .....	24
	Chapter 3. Stability of SAM at the Polymer Electrolyte/Lithium Metal Interface .....	35
	Chapter 4. Chemistry of Adsorption Process and the Ability of Different Adsorbed Molecules to Stabilize the Polymer Electrolyte/Lithium Metal Interface .....	50
	Chapter 5. Mechanism of Formation of Passivation Layer, With and Without Self-Assembled Monolayers.....	55
	Chapter 6. Scanning Probe AC Impedance Spectroscopy: A New Method to Study Electrode and Electrolyte Interfaces .....	61
VI.	Personnel Supported .....	72
VII.	Publications.....	72
VIII.	Participation/Presentations at Meetings, Conferences, Seminars, etc. ....	72
IX.	Consultative and Advisory Functions to Other Laboratories and Agencies .....	74
X.	Inventions, or patent Disclosures .....	74
XI.	Honors/Awards .....	74

## **I. Objectives of Work**

The proposed work involved the placement of self-assembled monolayers (SAMs) on the polymer electrolyte surface to deter and/or stabilize the formation of the passivation layer between the polymer electrolyte and the lithium electrode. This work combines two very scientifically and technologically important areas, lithium polymer batteries and self-assembled monolayers, resulting in a novel study with that has advanced the basic understanding of the electrode/electrolyte interface and the development of better battery systems. Specific objectives were as follows:

1. Determine the optimum conditions for the placement of self-assembled monolayers on polymer electrolyte surfaces.
2. Determine the SAM's ability to prevent passivation at the lithium/polymer electrolyte interface by electrochemical studies (cyclic voltammetry, a.c. impedance spectroscopy, battery cycling studies) and investigate the mechanism by which corrosion prevention occurs.
3. Investigate the structure of the self-assembled monolayers using FT-IR spectroscopy, Raman spectroscopy, scanning probe microscopy, surface energy studies, and the electrochemical techniques mentioned above.
4. Investigate the ion conduction mechanism through the non-polar hydrocarbon region of the self-assembled monolayers.

## **II. Executive Summary of Work**

A summary of the work accomplished in this study is given below. Each heading corresponds to the indicated chapter in the report, where more information about that topic can be found.

### **Chapter 1. Placement and Characterization of Self-Assembled Monolayers at the Electrode/Electrolyte Interface and the Ability of the Monolayer to Prevent Passivation**

The presence of self-assembled monolayers on the surface of PEO electrolyte films was verified by FTIR ATR spectroscopy. The monolayers were found to be very ordered and crystalline in nature. Nyquist plots of ac impedance spectroscopy of the PEO electrolyte films covered with the monolayers showed two semicircles. The second, low-frequency semicircle was determined to be due to the formation of a passivation layer at the interface. This was determined by comparison of impedance data for lithium symmetric cells and stainless steel symmetric cells. In the case of the stainless steel cells,

the second semicircle was absent, indicating that that this semicircle was due to passivation. Interestingly, the resistance of the bulk electrolyte was found to be less when the monolayer was present on the surface of the electrolyte. This seems to be contrary to what would be expected since the presence of the hydrocarbon tails would be expected to hinder conduction. Impedance tests done using mercury symmetric cells, which are able to conform to the surface of the electrolyte, show that this enhanced conduction was due to better molecular level contact caused by the self-assembled monolayer. This better contact offsets the reduction in ionic conduction caused by the hydrocarbon tails in the monolayer.

AFM data show that an adsorbed monolayer is indeed much smoother than the non-coated polymer surface. The orientation of the adsorbed layer was also seen to be perpendicular to the surface with the PEO portion of the adsorbed molecule adsorbing on the surface and the hydrocarbon tails stacked side-by-side. The ability of molecules, with different PEO segment lengths, to adsorb on the surface was investigated by FTIR. FTIR ATR spectra show that molecules with shorter PEO segments adsorb more readily.

## **Chapter 2. Chemistry of the Polymer Electrolyte/Lithium Metal Interface, With and Without Self-Assembled Monolayer Protection**

The passivation layer formed when lithium metal is in contact with PEO-triflate electrolyte has been investigated. Lithium surface films composed of grains and crystalline regions can be observed by AFM and current sensing AFM, (CSAFM). AFM and CSAFM images indicate that these films have low conductivities compared to lithium surfaces where passivation has been inhibited by the adsorption of self-assembled monolayers. ATR-FTIR studies of the lithium/polymer interface indicate that one of the first reactions in the passivation process at the lithium/polymer electrolyte interface is the formation of the  $\text{CF}_3$  radical, which quickly extracts a hydrogen atom from the polymer backbone. Somewhat later in the reaction scheme, lithium also begins to break the polymer chain at the C-O bond forming Li-O-R type compounds. Interestingly, it appears that many of the end groups resulting from these polymer chain-breaking reactions are of the form  $\text{CH}_3\text{-CH}_2\text{-}$ . This is one of the few characterizations conducted on the lithium electrode/polymer electrolyte interface in terms of the actual chemical species present. This study provides the background necessary to understand how adsorbed molecular layers inhibit passivation.

## **Chapter 3. Stability of SAM at the Polymer Electrolyte/Lithium Metal Interface**

SAMs used in this study, to temperatures at least as high as  $75^\circ\text{C}$ , are good at stabilizing the lithium metal/polymer electrolyte interface under open circuit conditions for periods of six days and longer. As discussed above, interface stabilization may primarily be due to the hydrocarbon tails of the SAM keeping the reactive lithium metal away from the polymer electrolyte surface where reactions with the PEO backbone and reactions with the lithium salt anion can easily occur, forming a passivation layer that is highly resistant to ion flow.

With cycling, there is some apparent degradation of the SAM layers which decreases the effectiveness of SAMs to stabilize the interface under extended time tests. This becomes evident by the increase in passivation resistance. However, even under cycling conditions for time periods as long as nine days, the passivation resistance for interfaces where the SAMs are present is always lower than interfaces that are not protected by the SAMs.

#### **Chapter 4. Chemistry of Adsorption Process and the Ability of Different Adsorbed Molecules to Stabilize the Polymer Electrolyte/Lithium Metal Interface**

Molecules having the general form  $R-(CH_2CH_2O)_m-H$  can adsorb on PEO polymer electrolyte surfaces. Adsorption of these molecules stabilize the lithium/polymer electrolyte interface whether the R group is a long, straight hydrocarbon tail capable of forming an ordered self-assembled structure or a branched hydrocarbon or a siloxane with bulky hydrocarbon groups that form a brush structure. The critical factor appears to be that the R group forms a continuous layer that does not allow the lithium to “see” the polymer electrolyte surface, thereby preventing reactions from occurring that can destabilize the interface. While an R-OH and an R-COOH, where R was a long, straight chain hydrocarbon, were found to adsorb on the surface, they did not stabilize the interface. This was attributed to a low adsorption density that resulted in the inability of the R groups to form a continuous protective molecular layer. These adsorbed molecular protective layers placed on “dry” polymer electrolytes, as studied here, or on gel polymer electrolyte systems have the potential to stabilize both the anode and cathode interfaces.

#### **Chapter 5. Mechanism of Formation of Passivation Layer, With and Without Self-Assembled Monolayers**

In the case where no SAM is present, the active surface area of passivation at the polymer electrolyte/lithium electrode interface decreases rapidly to about 60% in the first 48 hours after electrolyte/electrode contact. Then it plateaus at approximately 45%. This is consistent with the passivation layer growing rapidly initially and then forming a compact layer that remains relatively constant with time. To our knowledge, this is the first attempt at quantifying the extent of passivation in terms of the surface area rendered inactive. For the case of the interface protected by SAMs, it can be seen that the active surface area decreases to about 70% in 24 hours, but it recovers about 80% and no further deterioration of the surface is evident. The recovery is probably due to the rearrangement of surface molecules. It is evident from data collected that the interface changes little with time and remains stable due to the protection offered by SAMs present at the interface. Calculation of the sizes of active and inactive sites, as outlined earlier, reveals that the sites are of the order of a few tens of nanometers.

## **Chapter 6. Scanning Probe AC Impedance Spectroscopy: A New Method to Study Electrode and Electrolyte Interfaces**

AC impedance spectroscopy can be conducted at the nanoscale by combining this technique with atomic force microscopy. The surface of polymer electrolyte films was the object of this nanoscale study. It was shown that the AFM could differentiate regions of high and low ion-conductivity on the films. We compared the impedance data at the nanoscale with macroscale measurements and found no difference in the information obtained except for the magnitude of the impedance, with nanoscale measurements typically much larger than those at the macroscale. This was attributed to the large difference in area of the electrodes. After correcting for the size difference, nanoscale data were found to be consistent with macroscale data. Changing the force on the AFM probe was shown to have varying effects on impedance measurements. It was speculated that changes in the applied force cause changes in the tip/surface contact area, which in turn affects the impedance. It was shown that a.c. impedance data could be collected at the nanoscale. The work presented here shows the potential for this technique in the investigation of conductivity through specific surface sites and features. It is also possible to investigate the electrical properties of the surface of electrolytes and electrodes on the nanoscale.

### **III. Significance of Work**

This work has shown the potential for molecular self-assembly to stabilize the interfaces important to lithium/polymer electrolyte systems. It seems reasonable to assume that this technology could also be used to stabilize the cathode/electrolyte interface. It also should be amenable to plasticized and gel polymer electrolyte systems, perhaps eventually making them more suited for use with solid lithium electrodes. This technique appears to be an example where nanotechnology is able to live up to its promised significance and solve macroscopic problems of technical importance.

### **IV. Technical Issues to be Addressed in the Future**

There are two areas that must be investigated if SAM technology is to reach its full potential in battery technology. First, the increase in the charge transfer resistance caused by the blocking nature of the SAMs must be addressed. One way to approach this is to shorten the length of the hydrocarbon tails of the molecules used to make the SAMs, which will presumably make charge transfer easier. However, a trade-off between the ability of the SAM to stabilize the interface and a decrease in charge transfer resistance will probably result. Research is being conducted in our laboratory where interface stabilization and ease of charge transfer are being maximized by changing the chemical make-up of the molecules used to make the SAM. The second area of concern is the stability of the SAM under cycling conditions. Likewise, this factor may also be able to be addressed by the chemistry of the molecules used to make the SAM. Previous work in our laboratory has shown that molecules having groups such as poly(dimethyl siloxanes) and branched hydrocarbon chains can be adsorbed onto the polymer surface. While these

molecules when adsorbed on the surface of the polymer electrolyte may not form the ordered, self-assembled structures like those studied here, they do form self-assembled molecular “brush” layers that are nevertheless densely backed enough to stabilize the lithium/electrolyte interface. Thus, because of the numerous chemistries that can be tried, SAMs of appropriate chemical composition may be found that will better withstand battery cycling. Changing the chemical make-up of the SAMs seems to present many interesting opportunities to maximize their performance and to better understand their mechanism of stabilization.



## **Chapter 1. Characterization of Self-Assembled Monolayers at the Electrode/Electrolyte Interface and the Ability of the Monolayer to Prevent Passivation**

### **1.1 Introduction**

It is widely accepted that the formation of passivating layers can affect the performance of polymer electrolyte cells, and it has been shown that interfacial impedance in lithium/polymer electrolyte systems can grow with time until it is significantly larger than the bulk resistance [1,2]. Techniques of minimizing certain reactions at the electrode/electrolyte interface could thus be beneficial to lithium polymer battery development. Some researchers have approached this problem by studying and modifying the lithium metal surface [2-6]. However, the polymer electrolyte surface is a much easier surface to work with than the extremely reactive lithium surface; and recent studies conducted in our laboratory [7] have indicated that self-assembled molecular layers placed on the polymer surface can offer protection from passivation and appear to have the potential to protect the interface and enhance cell performance. Our previous work using a.c. impedance spectroscopy has shown that the wax  $\text{H}-(\text{CH}_2)_{32}-(\text{CH}_2-\text{CH}_2-\text{O})_{10}-\text{H}$  adsorbed on PEO electrolyte surfaces greatly slows the formation of a passivation layer in lithium symmetric cells stored under an open circuit potential [7]. A proposed structure of the adsorbed film was a self-assembled molecular layer of the type shown in Figure 1.1.

This structure can be rationalized if one assumes that the amorphous poly(ethylene oxide)-like portion of the wax molecule,  $(\text{PEO})_m$  region, preferentially orients itself to absorb onto the poly(ethylene oxide) electrolyte film. This leaves the polyethylene-like  $\text{CH}_2$  segment,  $(\text{PE})_n$ , of the wax molecule to self-assemble into an ordered layer just above the electrolyte surface. The ordered nature of the  $(\text{PE})_n$  tail was determined by ATR-FTIR spectroscopy by observation of the  $700\text{-}800\text{ cm}^{-1}$  region of the infrared spectrum which is the area where the  $\text{CH}_2$  rocking mode should occur. The  $\text{CH}_2$  rocking mode for  $(\text{CH}_2)_4$  and longer hydrocarbon chains is found in this region and is known to "split" into two peaks appearing at approximately  $720$  and  $730\text{ cm}^{-1}$  due to the crystal field effects of crystalline polyethylene [8]. ATR-FTIR spectra for PEO electrolyte films with  $\text{H}-(\text{CH}_2)_{32}-(\text{CH}_2-\text{CH}_2-\text{O})_{10}-\text{H}$  adsorbed on the surface exhibited these two modes, indicating that the adsorbed surface layer had a very ordered hydrocarbon chain. The crystal field splitting of the  $\text{CH}_2$  mode observed in the infrared spectrum would indicate that such an orderly arrangement exists, resulting in a crystalline environment.

This section of the report is concerned with the further investigation of the ability of self-assembled molecular layers to reduce passivation at the  $\text{Li}/\text{polymer}$  interface, how these layers may adsorb, and their structure.

### **1.2. Experimental**

#### **1.2.1. Film preparation**

All films were made with a 15:1 ratio of ether oxygen to lithium. Films were prepared in an argon atmosphere as described previously [7] and were dried and stored at 50°C in a vacuum oven. The thickness of the films ranged from 60 to 80  $\mu\text{m}$ . Semicrystalline waxes from Petrolite Specialty Polymers, which could best be described as  $\text{H}-(\text{CH}_2)_n-(\text{CH}_2\text{CH}_2\text{O})_m\text{H}$  (later abbreviated as  $(\text{PE})_n-(\text{PEO})_m$ ) were used to form self assembled molecular layers on the polymer surface. This was accomplished via adsorption. One pure hydrocarbon wax having the formula  $\text{H}-(\text{CH}_2)_{29}\text{H}$ , or  $(\text{PE})_{29}$ , was also used in adsorption studies. The chemical formulas of all waxes used are given in Table 1. Concentrated solutions of the different waxes were prepared in Fisher Optima Grade hexane and a selected electrolyte film was placed in the solutions and allowed to equilibrate for at least 72 hours. Shorter equilibrium times did not result in good molecular formation. The film was removed and quickly rinsed in pure hexane to remove wax that might deposit from evaporation of the hexane-wax solution. Films not receiving molecular layers were soaked in neat hexane for an equal period of time in order to make certain that all films were treated similarly. These films were dried and stored at 50°C in a vacuum oven.

### 1.2.2. Apparatus

Surface infrared spectra, using the Attenuated Total Reflection (ATR) technique, were collected on a Nicolet 510P Fourier Transform Infrared Spectrometer with a DTGS detector at  $1\text{ cm}^{-1}$  spectral resolution. The ATR-FTIR spectra were obtained by using a Spectra-Tech Horizontal Contact Sampler ATR with a flat plate cell and a ZnSe crystal cut at 45°. The average depth of penetration of the infrared radiation was calculated by using the following equation

$$d_p = \frac{\lambda}{2\pi n_1 (\sin^2 \theta - n_{21}^2)^{1/2}}$$

where  $d_p$  is the depth of penetration,  $\lambda$  is the wavelength of the radiation in air,  $\theta$  is the angle of incidence ( $= 45^\circ$ ),  $n_1$  is the refractive index of the ATR crystal ( $= 2.4$ ),  $n_{21}$  is the ratio of the refractive index of the sample to that of the ATR crystal ( $= 0.605$ ). The average depth of infrared radiation penetration into the sample in the region of interest was found to be approximately  $1.0\text{ }\mu\text{m}$ . The films to be studied were quickly removed from their vacuum oven, placed on the plate, and sealed with a rubber cover of the Contact Sampler apparatus. This ATR sampling arrangement was used so that the films could be protected from water in the atmosphere.

An HP 4194-A a.c. impedance/gain phase analyzer was used to investigate the electrochemistry of symmetric lithium, stainless steel, and mercury cells. This was done over a range of 40MHz to 100Hz. Test cells for impedance analysis were assembled in a glove box under argon purge. The lithium cells were stacked by hand in the following order: stainless steel, lithium, electrolyte film, lithium and stainless steel. The lithium was omitted in the stainless steel cells. The stack was then clamped and inserted into a glass

tube that was sealed and placed under vacuum. Mercury cells were made by using two right angle bent glass tubes with one half of a O-Ring joint at the end of each tube. A viton o-ring was used in the joints to ensure sealing. The films to be studied were placed between the two halves of the joint and clamped in place. Each tube was then filled with mercury and sealed with a glass cap. Contact to the HP 4194-A impedance/gain phase analyzer was made by wires from the analyzer running through the glass cap by means of a metal-glass seal into the mercury. A silicon oil bath was used to maintain the temperature of all cells at  $50 \pm 1$  °C.

To gain more information about the film surface, light microscopy and atomic force microscopy (AFM) were also used. Both experiments were performed on samples which had been mounted on glass microscope slides with double-sided adhesive tape. An Olympus BH2 microscope was used to obtain the light microscopic features of the surface by light reflection. AFM (topography and phase) images were recorded with a PicoSPM (Molecular Imaging, Tempe, AZ, USA) microscope, operated in Magnetic AC mode (MAC mode<sup>TM</sup>, i.e. "Tapping" mode) with a 85  $\mu\text{m}$  triangular MAClever cantilever. AFM experiments were carried out in an environmental chamber under nitrogen to avoid water contamination of the hygroscopic films.

### 1.3. Results and Discussion

#### 1.3.1. Presence of self-assembled molecular layers

The presence of the adsorbed molecular layers was determined by ATR-FTIR spectroscopy as done in previous work [7]. This was done by investigating the  $\text{CH}_2$  rocking mode region. All spectra (not shown here) of PEO films having been exposed to solutions of waxes that have the  $(\text{PEO})_m$  segments listed in Table 1 exhibited modes at 720 and 730  $\text{cm}^{-1}$ , indicating that ordered, crystalline molecular layers of  $(\text{PE})_n$  were formed. Interestingly, films where the  $(\text{PE})_{29}$  wax was used for adsorption had no peaks in this region, pointing out that no adsorption occurs for this molecule. This indicates that all the waxes with the  $(\text{PEO})_m$  tails can adsorb on the surface, forming ordered self-assembled  $(\text{PE})_n$  regions. The one wax without the  $(\text{PEO})$  tail,  $(\text{PE})_{29}$ , was not able to adsorb.

Table 1 - Chemical and abbreviated formulas of waxes studied.

Chemical Formula	Abbreviated Formula
$\text{H}(\text{CH}_2)_{32}-(\text{CH}_2\text{CH}_2\text{O})_{2-3}\text{H}$	$(\text{PE})_{32}-(\text{PEO})_{2-3}$
$\text{H}(\text{CH}_2)_{32}-(\text{CH}_2\text{CH}_2\text{O})_{10}\text{H}$	$(\text{PE})_{32}-(\text{PEO})_{10}$
$\text{H}(\text{CH}_2)_{32}-(\text{CH}_2\text{CH}_2\text{O})_{41}\text{H}$	$(\text{PE})_{32}-(\text{PEO})_{41}$
$\text{H}(\text{CH}_2)_{40}-(\text{CH}_2\text{CH}_2\text{O})_3\text{H}$	$(\text{PE})_{40}-(\text{PEO})_3$
$\text{H}(\text{CH}_2)_{40}-(\text{CH}_2\text{CH}_2\text{O})_{12-13}\text{H}$	$(\text{PE})_{40}-(\text{PEO})_{12-13}$
$\text{H}(\text{CH}_2)_{29}\text{H}$	$(\text{PE})_{29}$

### 1.3.2. A.c. impedance data showing passivation protection

A.c. impedance data for lithium symmetric cells were collected over varying time ranges for PEO electrolyte films and PEO electrolyte films with the waxes listed in Table 1 adsorbed on the surface. Some of these data expressed as Nyquist plots are shown in Figure 1.2. The data for the film without the wax (upper plot in Figure 1.2) shows two overlapping semicircles present after 18 hours in the lithium symmetric cell at open circuit voltage. The capacitance of these semicircles was estimated by knowing that the maximum of each semicircle obeys the relation  $\omega RC = 1$ . The first semicircle has a capacitance in the range of pF usually associated with the bulk response, while the second has a value in the range of  $10^{-8}$  F indicating the response of a passivating film at the Li/polymer electrolyte interface [9]. The second semicircle is found to initially grow with time and perhaps start decreasing at longer times, though limitation in the frequency range makes it difficult to rule out that a second larger semicircle is appearing at much lower frequencies. The initial increase in what appears to be interface passivation, followed by a decrease, has been observed before at the Li/polymer electrolyte interface [6] and has been attributed to the change in the structure of the passivation layer with time to a slightly better ion conducting layer. This could be happening in these data. The lower Nyquist plots illustrate that adsorbing a molecular layer on the electrolyte films appears to prevent the formation of the second semicircle associated with the passivation layer. All the waxes listed in Table 1 when adsorbed on the polymer electrolyte surface exhibited similar behavior except for two. PEO films where adsorption of the (PE)<sub>29</sub> wax was attempted had Nyquist plots that were similar to films that had no exposure to adsorbing molecules. This is not surprising as IR data discussed earlier in this paper indicated that this wax without a (PEO)<sub>m</sub> tail does not adsorb on the surface of the PEO electrolyte film. We also have not collected consistent data for the (PE)<sub>32</sub>-(PEO)<sub>41</sub> wax at this time.

In order to better confirm that our interpretation of the Nyquist plots was correct, studies were conducted where the lithium non-blocking electrodes were replaced with symmetric stainless steel blocking electrodes. Data for two films are shown in Figure 1.3. Here we see only one semicircle, which must be due to the bulk capacitance for both the film with an adsorbed layer and the one without. The bulk resistance of the two films, as estimated by the intercept of the semicircle with the x axis, also compares well with similar values for the lithium non-blocking electrodes. This seems to confirm that the first semicircle in the lithium cells is due to bulk capacitance while the second is a passivation layer formed due to contact with the reactive, non-blocking lithium electrode.

Two unusual trends are seen for the capacitance of the bulk electrolyte (first semicircle). With time the capacitance is seen to increase slightly for the bulk. We attribute this to change in the crystalline nature of the bulk PEO. These studies have been conducted at 50°C, which is below the 65°C melting temperature of crystalline PEO but is most likely in an optimum range for crystallite formation. With time, the percent of crystallinity may increase, slightly lowering the bulk conductivity.

The second trend is that PEO electrolyte films with surface molecular layers have a higher conductivity than those without, which was also seen in our previous studies [7].

Lithium ion movement through the ordered  $(PE)_n$  tails would be difficult, so one must assume that the  $(PE)_n$  layer shown in Figure 1.1 would have defects through which ions could move. However, it is difficult to explain how the ion conductivity could actually be enhanced. One possibility is that the molecular layers on the surface of the electrolyte provide better contact with the solid lithium surface, perhaps because of a molecular smoothing effect or because of easier deformation of this molecular layer to make better contact with the lithium electrode. One way to investigate this is to use non-blocking mercury electrodes, which, because of their liquid state, should be able to conform to a polymer electrolyte surface with or without the molecular layers. Figure 1.4 shows Nyquist plots for such cells. Here the trend is reversed with the PEO electrolyte film with the adsorbed wax molecular layer having a higher resistance than the film without the molecular layer. Intuitively this is what one would expect, and the higher conductivity in lithium symmetric cells would seem to be due to better contact of the lithium with the surface, either by smoothing of the PEO electrolyte surface or by making a surface that more easily conforms to the lithium electrode surface. This demonstrates the importance of electrode/electrolyte contact.

### 1.3.3. Light microscopy and AFM characterization of molecular layers

The surface of the films was further investigated using both light microscopy and AFM. Figure 1.5 is the light microscope image of the surface of a PEO electrolyte film without a molecular layer. The large circular structures are spherulites at the surface of the polymer with crystalline lamellae radiating from their centers. Figure 1.6 is a PEO electrolyte surface with  $(PE)_{40}$ - $(PEO)_3$  adsorption, which is the typical appearance for all waxes adsorbed on the electrolyte surface. The adsorption of the wax can be seen to cover the spherulitic structure, perhaps smoothing the surface. A better understanding of the structure of the adsorbed layers can be obtained by AFM studies. Figure 1.7 shows the AFM image of PEO film without an adsorbed layer (top) and with the adsorbed layer (bottom) of  $(PE)_{32}$ - $(PEO)_{10}$ . For both films the topography image is on the left with the phase image on the right. The lamellar structure of the spherulite can be seen in the film without the adsorbed layers. The average height of the lamellae seen in these images is  $2.5 \pm 0.5$  nm. Images showing the adsorbed layer are quite different than those without this layer. The surface appears to be much smoother with the lamellae having been covered by adsorbed wax. What seem to be the edges of layers that in some cases define "islands" are observed. The average height of the layers was found to be  $5.5 \pm 0.5$  nm.

We attribute these layers to adsorbed molecules of the  $(PE)_{32}$ - $(PEO)_{10}$  wax. Assuming that the structure of the adsorbed layer is as pictured in Figure 1.1, some interesting comparisons can be made. Crystalline polyethylene's unit cell is known to have a chain axis length of 0.253 nm with two repeating units per cell [11]. Using this value the length of the  $(PE)_{32}$  portion of the  $(PE)_{32}$ - $(PEO)_{10}$  molecule would be approximately 3.9 nm. Assuming the  $(PEO)_{10}$  portion of the molecule has the typical helical structure found in its crystalline unit cell, one repeating unit would have a length of 0.2783 nm [12-14] resulting in this portion of the molecule having a length of 2.8 nm. Thus the total calculated length of this molecule, if it were adsorbed on the surface by attachment of one end and in an extended configuration such as shown in Figure 1.1

would be approximately 5.7 nm. This distance can be compared with the observed layer edge height of  $5.5 \pm 0.5$  nm. It is felt that the layer edge height observed in this work corresponds to monolayers of  $(\text{PE})_{32}$ - $(\text{PEO})_{10}$  molecules adsorbed vertically on the surface. The difference between the calculated height and the observed value could be due to the  $(\text{PE})_{32}$  portion of the chain having a slight tilt from  $90^\circ$  orientation. Work on self-assembled monolayers on metal surfaces indicates that tilt angles from the surface normal for the hydrocarbon chains vary from 12 for densely packed layers to 30 degrees for those not as tightly packed [15]. If the  $(\text{PE})_{32}$  portion of the wax molecule was tilted in such a manner, a value closer to the observed 5.5 nm would be expected.

A monolayer structure could be an oversimplification, since this adsorption could be a multilayer type system with the first layer being similar to that shown in Figure 1.1. A second layer would adsorb on top of the first layer with the molecular orientation being inverted so the  $(\text{PE})_{32}$  portion of the adsorbing molecule would be in contact with the  $(\text{PE})_{32}$  portion of the first layer. Adsorption would continue in this alternating pattern forming multilayers. This process would explain the ability of the wax to completely cover the relatively rough surface of the PEO electrolyte film, smoothing it not only on the molecular level, but on a more macroscopic level as seen in light microscopy images.

#### 1.3.4. ATR-FTIR studies of the adsorption process

While data have shown that molecular layers can adsorb on the surface of PEO electrolyte films and that they help prevent passivation, it has also been demonstrated that the pure hydrocarbon  $(\text{PE})_{29}$  will not adsorb. Thus, the understanding of the factors involved in adsorption would appear to be important. The adsorption of these compounds was further studied by investigation of the  $\text{CH}_2$  stretching region of the IR spectra. These ATR-FTIR data are shown in Figure 1.8 for the pure wax  $(\text{PE})_{32}$ - $(\text{PEO})_{10}$  and the PEO electrolyte film not exposed to adsorbing waxes. The dominant feature in this region for the waxes is the  $\text{CH}_2$  symmetric and asymmetric stretch observed at 2848 and  $2916 \text{ cm}^{-1}$  respectively that are due to the long  $(\text{PE})_n$  chains of the wax. The films with adsorption also show a small mode at  $2887 \text{ cm}^{-1}$  due to the  $\text{CH}_2$  stretch of the  $(\text{CH}_2\text{-CH}_2\text{-O})$ , i.e.  $(\text{PEO})_m$  region of the wax molecule. The dominant mode in the PEO film is the same  $\text{CH}_2$  stretch except that the frequency has been lowered to  $2882 \text{ cm}^{-1}$ . The 2848 and  $2916 \text{ cm}^{-1}$  modes are not seen in the PEO film because there is no long  $\text{CH}_2$  chain present.

An indication of the ability of the waxes to adsorb on the surface can be obtained by comparing the ratio of the intensities of the strong mode at  $2916 \text{ cm}^{-1}$  of the waxes with the  $2882 \text{ cm}^{-1}$  mode of the PEO electrolyte film. For the series of waxes all having the same  $(\text{PE})_{32}$  hydrocarbon tail, this ratio for the  $(\text{PEO})_{2-3}$ ,  $(\text{PEO})_{10}$  and  $(\text{PEO})_{41}$  is roughly 3:2:1, which indicates that the shorter the  $(\text{PEO})_m$  portion of the molecule, the more wax that can adsorb on the surface. ATR-FTIR data (not shown here) for the two waxes  $(\text{PE})_{40}$ - $(\text{PEO})_{10}$  and  $(\text{PE})_{40}$ - $(\text{PEO})_{41}$  adsorbed on the PEO surface show a similar trend with ratios of 4:1 respectively. It appears that short  $(\text{PEO})_m$  segments are more conducive to molecular adsorption, yet the  $(\text{PE})_{29}$  with its absence of the  $(\text{PEO})_m$  part of the molecule results in no adsorption. Shorter  $(\text{PEO})_m$  segments may simply be able to adsorb better due to less opportunity of the shorter segments to be disorderedly adsorbed

on the surface. Longer segments may find it difficult to properly adsorb and at the same time allow self-assembly of the  $(PEO)_n$  segments. Another factor could be the solubility of the waxes. Waxes with shorter  $(PEO)_n$  segments are more soluble in hexane. The increased solubility of a wax could certainly enhance the chances for adsorption to occur.

#### 1.4. Conclusions

The presence of self-assembled monolayers on the surface of PEO electrolyte films was verified by FTIR ATR spectroscopy. The monolayers were found to be very ordered and crystalline in nature. Nyquist plots of ac impedance spectroscopy of the PEO electrolyte films covered with the monolayers showed two semicircles. The second, low frequency semicircle was determined to be due to the formation of a passivation layer at the interface. This was determined by comparison of impedance data for lithium symmetric cells and stainless steel symmetric cells. In the case of the stainless steel cells, the second semicircle was absent indicating that that this semicircle was due to passivation. Interestingly, the resistance of the bulk electrolyte was found to be less when the monolayer was present on the surface of the electrolyte. This seems to be contrary to what would be expected since the presence of the hydrocarbon tails would be expected to hinder conduction. Impedance tests done using mercury symmetric cells, which are able to conform to the surface of the electrolyte, show that this enhanced conduction was due to better molecular level contact caused by the self-assembled monolayer. This better contact offsets the reduction in ionic conduction caused by the hydrocarbon tails in the monolayer.

AFM data show that adsorbed monolayer is indeed much smoother than the non-coated polymer surface. The orientation of the adsorbed layer was also seen to be perpendicular to the surface with the PEO portion of the adsorbed molecule adsorbing on the surface and the hydrocarbon tails stacked side-by-side. The ability of molecules with different PEO segment lengths to adsorb on the surface was investigated by FTIR. FTIR ATR spectra show that molecules with shorter PEO segments adsorb more readily.

#### 1.5. References

1. P. G. Bruce and F. Krok, *Solid State Ionics*, **36**, 171 (1989).
2. P. G. Bruce and F. Krok, *Electrochim. Acta* **33**, 1669 (1988).
3. J.L. Goldman, R.M. Mank, J.H. Young and V.R. Koch, *J. Electrochem. Soc.* **127**,1461 (1980).
4. V.R. Koch, J.L. Goldman, C.J. Mattos and M. Mulvaney, *J. Electrochem. Soc.* **129**, 1 (1982).
5. K.M. Abraham, J.S. Foos and G.L. Goldman, *J. Electrochem. Soc.* **131**, 2197 (1984).
6. Z.I. Takehara, Z. Ogumi, K. Kanamura and Y. Uchimoto in *Proceedings of the Symposium on Lithium Batteries*, Volume 94-4, The Electrochemical Society, Pennington, NJ p.13, (1994).
7. R. N. Mason, M. Smith, T. Andrews, and D. Teeters, *Solid State Ionics* **118**,129 (1999).

8. J.L. Koenig, in *Spectroscopy of Polymers*, American Chemical Society, Washington, D.C., 105 (1992).
9. P. G. Bruce in *Polymer Electrolyte Reviews* Volume 1, (Edited by J. R. MacCallum and C. A. Vincent) p. 237, Elsevier, London (1987).
10. C.A.C. Sequeira and A Hooper, *Solid State Ionics* **9-10**, 1131 (1983).
11. U. W. Gedde in *Polymer Physics*, p. 133. Chapman & Hall, London (1995).
12. Y. Takahashi and H. Tadokoro, *Macromolecules* **6**, 672 (1973).
13. A. Aabloo and J. Thomas, *J. Comput. Theor. Polym. Sci.* **7**, 47 (1998).
14. S. Nettesheim, D. Zeisel, M. Handschuh, and R. Zenobi, *Langmuir* **14**, 3101 (1998).
15. G. K. Jennings, J. C. Munro, T.-H. Yong, and P. E. Laibinis, *Langmuir* **14**, 6130 (1998).



1.6. Figures

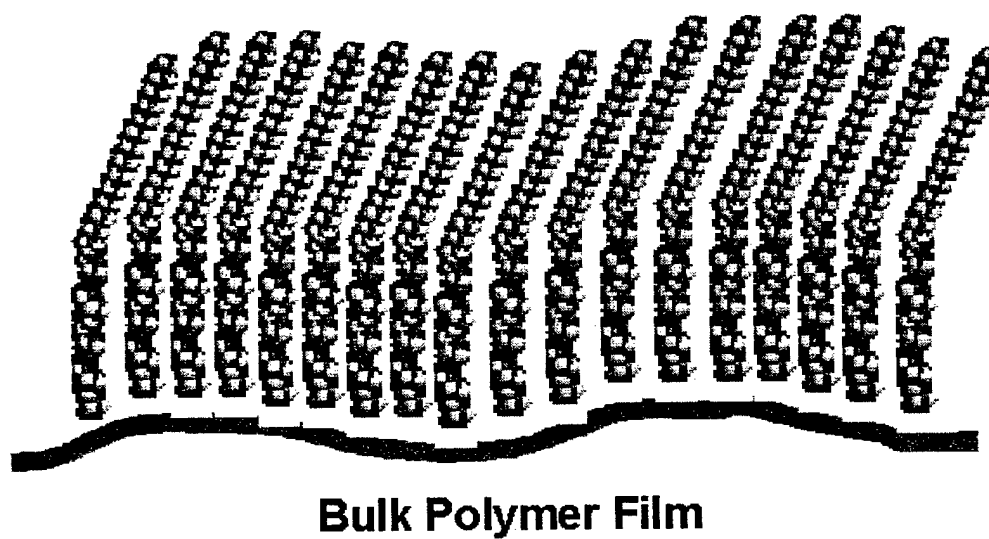


Figure 1.1

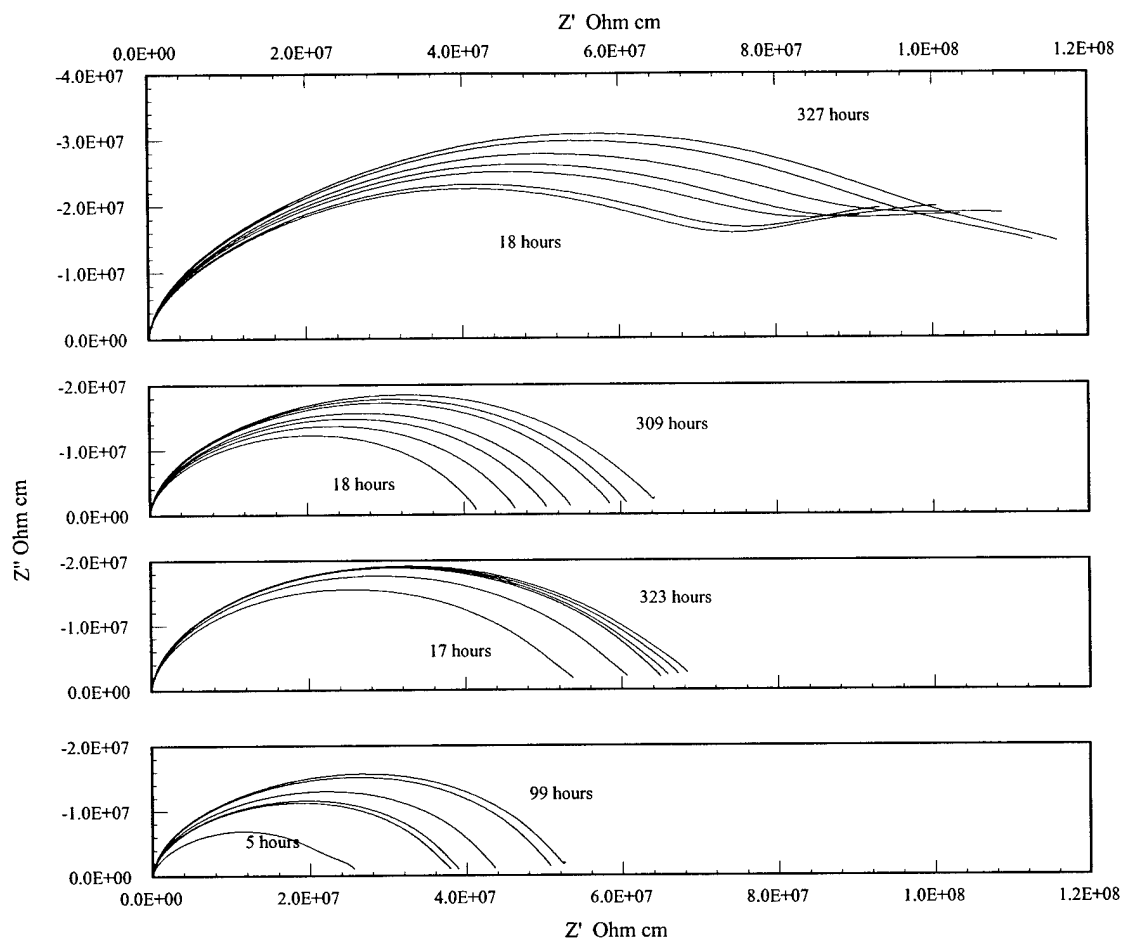


Figure 1.2

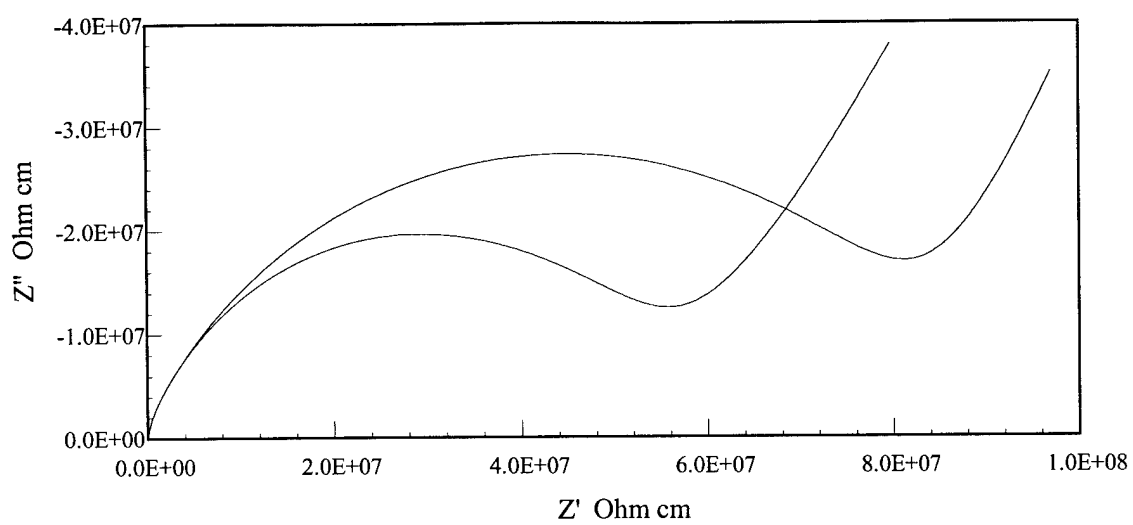


Figure 1.3

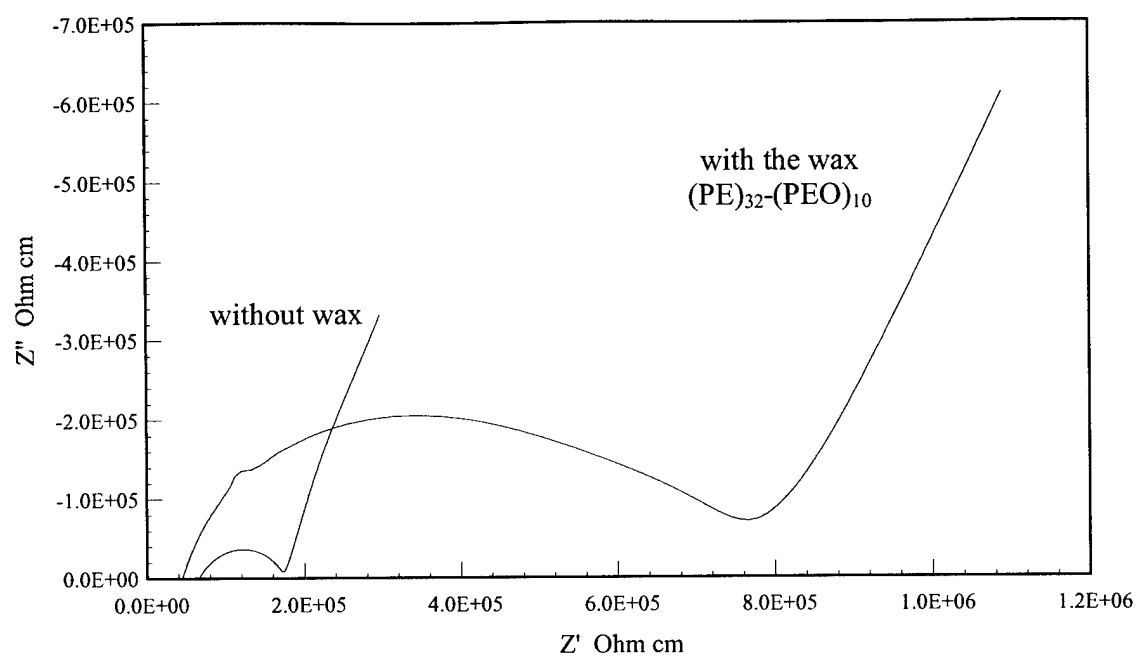


Figure 1.4

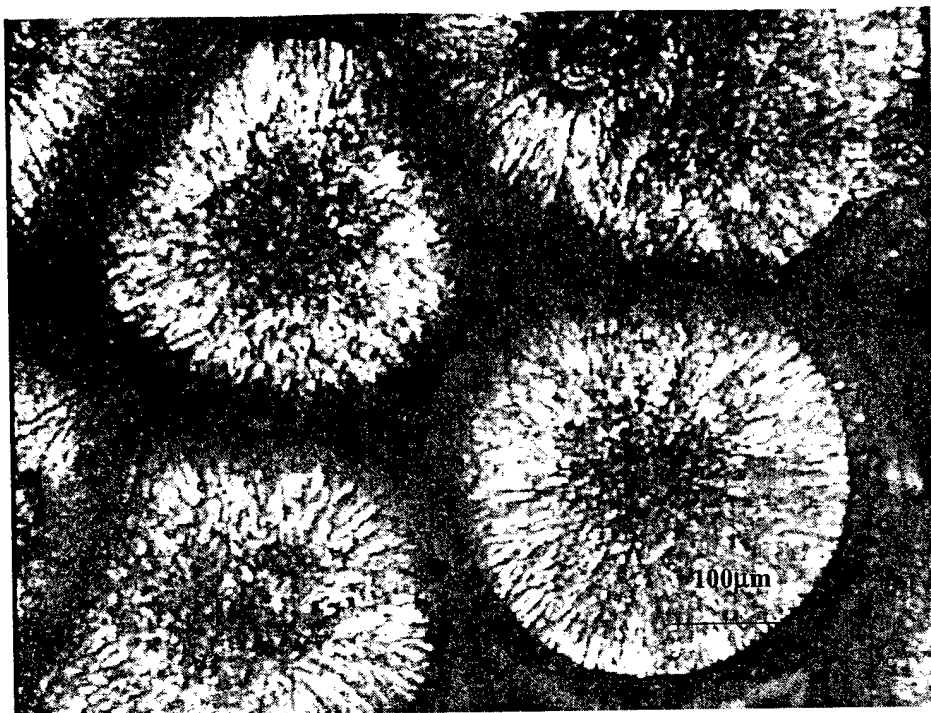


Figure 1.5

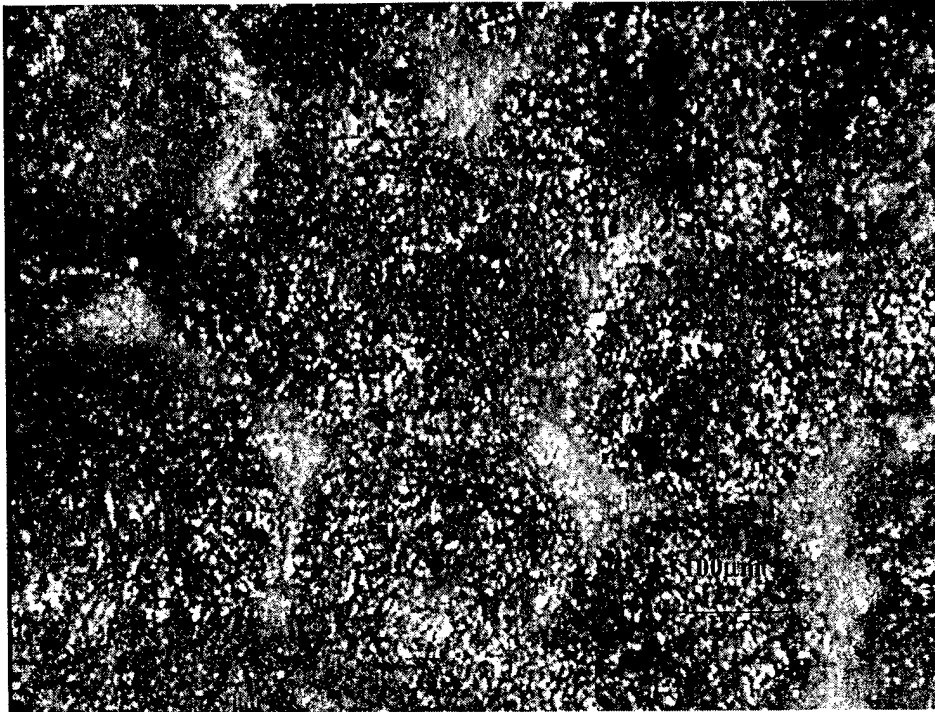


Figure 1.6

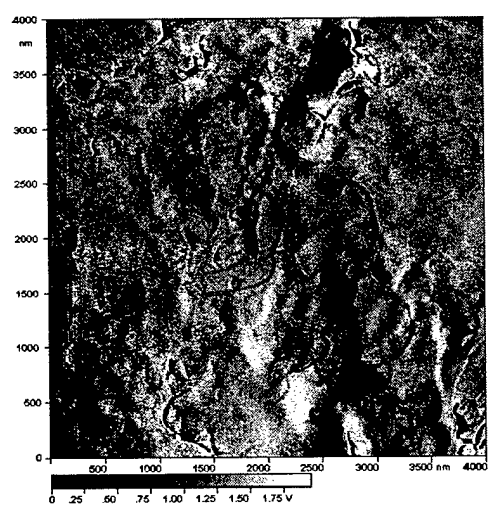
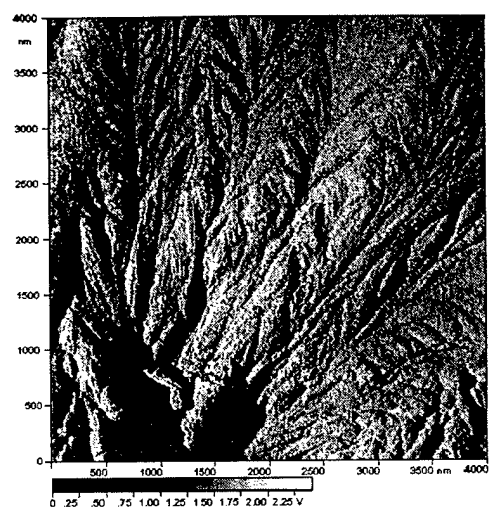


Figure 1.7

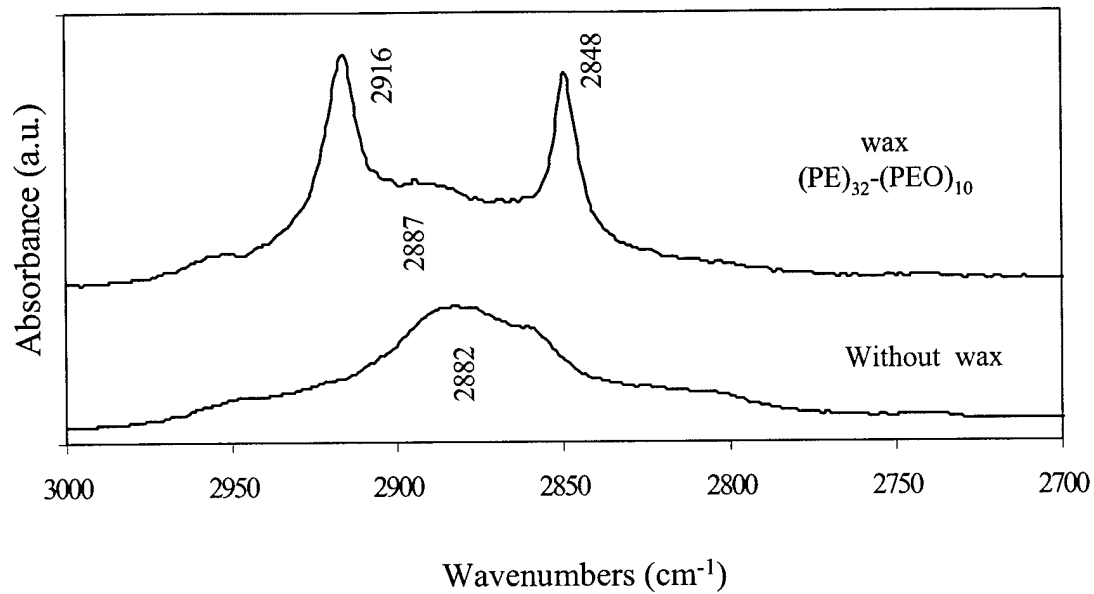


Figure 1.8



## **Chapter 2. Chemical Characterization of the Passivation Layer at the Lithium Electrode/Polymer Electrolyte Surface with and without Self-Assembled Monolayer Protection**

### **2.1. Introduction**

The formation of a passivation layer at the interface of lithium/polymer electrolyte systems is usually considered similar, from an electrochemical point of view, to lithium in liquid organic electrolytes. These lithium-liquid systems are well characterized [1]; however, the lithium polymer electrolyte interface, even though it has been the subject of electrochemical studies such as those given above, is simply not well understood. For instance the composition of these passivation films is certainly of importance, but it is the subject of some controversy. Fauteux [2] proposed that the reaction of lithium with poly(ethylene oxide) (PEO) complexed with lithium triflate  $\text{LiSO}_3\text{CF}_3$  resulted in the formation of  $\text{LiF}$  in the passivation layer. However, Vincent [3], based on the strength and stability of the C-F bond in comparison to the weaker C-S bonds in the triflate ion, proposed that lithium sulfite and  $\text{CF}_3$  radicals would be formed due to contact of lithium metal with the triflate salt. Lithium sulfite would be one of the major chemical species and the fluorocarbon radical would abstract a hydrogen atom from the polymer backbone resulting in the formation of  $\text{HCF}_3$ . Another important reaction at this interface is the chemical reaction of lithium with the polymer backbone itself. In this light, glyme-type compounds in contact with lithium have been used to model the lithium/polymer electrolyte interface by Aurbach's group [4,5] and Lisowska-Oleksiak [6]. Lithium compounds of the form of  $\text{Li-O-R}$  or  $\text{Li-O-R-O-Li}$  were observed by IR spectroscopy at the interface [4,5] and the formation of this film was associated with a passivation layer that was found to increase with time as the reaction with the glymes proceeded [6]. While Raman spectroscopy has been used to investigate the composition of salts in polymer electrolytes at the interface and through the bulk electrolyte [7], only preliminary work done by Kerr et al. [8] has looked at the chemical species actually formed at the lithium/polymer electrolyte interface.

The work presented in this portion of the report involves the characterization of the passivation layer between lithium and PEO-lithium triflate electrolytes using attenuated total reflection (ATR) FTIR spectroscopy and atomic force microscopy (AFM) having current-sensing capabilities. In addition, the lithium electrode/polymer electrolyte interface will be probed by inhibiting the passivation layer by using self-assembled molecular layers on the polymer electrolyte surface. The use of these molecular layers for passivation prevention in lithium/polymer electrolyte systems has been described in Chapter 1 of this report.

### **2.2. Experimental**

#### **2.2.1 Film preparation**

All films were made by using poly(ethylene oxide) and lithium triflate (Aldrich) with a 15:1 ratio of ether oxygen to lithium. Films were prepared in an argon atmosphere and were dried and stored at 50°C in a vacuum oven. Semicrystalline wax from Petrolite Specialty Polymers, described as  $\text{H}-(\text{CH}_2)_{32}-(\text{CH}_2-\text{CH}_2-\text{O})_{10}-\text{H}$ , was used to form self-assembled molecular layers on the polymer surface. This was accomplished via adsorption. The complete procedure for film preparation and formation of the self-assembled molecular layers on the film has been described previously in this report.

### 2.2.2. Apparatus

Surface infrared spectra, using the ATR technique, were collected on a Nicolet 510P Fourier Transform Infrared Spectrometer with a DTGS detector at  $1\text{ cm}^{-1}$  spectral resolution. The average depth of penetration of the infrared radiation was calculated as described previously and was found to be approximately  $1.0\text{ }\mu\text{m}$ . Time-dependent studies of the lithium/polymer interface under open circuit conditions were carried out with a Horizontal Contact Sampler ATR with a trough-shaped cell and a ZnSe crystal cut at  $45^\circ$ . Polymer films were coated on the crystal by evaporation of an appropriate concentration and volume of an acetonitrile solution of PEO/ $\text{LiSO}_3\text{CF}_3$  under nitrogen to obtain a film thickness of less than  $1\text{ }\mu\text{m}$ . A foil of lithium metal was brought in contact with the polymer film, and the ATR trough was sealed to prevent air contamination. Because the PEO film was less than  $1\text{ }\mu\text{m}$  in thickness, the infrared radiation beam could penetrate the film and reach the lithium/polymer interface. A diagram of the ATR experiment is shown in Figure 2.1.

To gain more information about passivation of lithium surfaces, atomic force microscopy (AFM) was used. Experiments were performed on lithium samples, which had been in contact with polymer electrolyte films. The lithium for this study was obtained by carefully “pulling apart” the lithium and polymer electrolyte sheets in lithium symmetric cells. The films separated easily and no apparent damage was done to the lithium surface. AFM images were recorded with a PicoSPM (Molecular Imaging, Tempe, AZ, USA) microscope, operated in contact mode and in current sensing mode (CSAFM). When using the current sensing mode a Pt coated cantilever was used, which simultaneously probes the conductivity and the deflection of the sample surface. A potential ranging from  $-0.5$  to  $+5.0$  volts was applied to the tip so that current through the sample can be measured. All samples were prepared and all cells assembled in an argon atmosphere glove box and AFM experiments were carried out in an environmental chamber under argon. a.c. impedance data was collected using a HP 4194A Impedance/Gain Phase Analyser.

## 2.3 Results and Discussion

Figure 2.2 is a Nyquist plot of the a.c. impedance data for the lithium symmetric cells where one has a self-assembled monolayer and passivation stabilization and the other does not have a SAM. As discussed previously in Chapter 1 in this report, self-assembled monolayers on the polymer electrolyte surface appear to inhibit passivation at the Li/electrolyte interface. This can be seen in these data as the film with the monolayers

does not have the second low frequency semicircle which is associated with the passivation layer [2,6]. Thus two systems, one with passivation and one where passivation has been inhibited, were available for study.

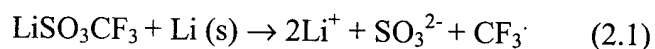
AFM images of the various surfaces studied are shown in Figure 2.3. Figure 2.3a is the surface of the lithium ribbon before contact with the polymer electrolyte. Elliptical grains that have an average size of 100 nm are observed. This appears similar to previous AFM images obtained by Morigaki and Ohta [8] of pristine lithium surfaces in dry atmospheres. Figure 2.3b is the lithium surface that has been in contact with the polymer electrolyte with adsorbed self-assembled monolayers. While some grains do seem to be expanded and what appear to be small crystals are present on the surface, this surface looks similar to the pristine lithium surface shown in Figure 2.3a. Thus it is not surprising that a passivating layer is not observed in the a.c. impedance data shown in Figure 2.2 for the film with the SAM. In some respects the self-assembled monolayers on the polymer electrolyte may act as a solid electrolyte interphase (SEI) minimizing the direct reaction between the lithium metal and the polymer electrolyte. CSAFM data for this lithium surface are shown in Figure 2.3c. The entire surface shows reasonable conductivity with the highest conductivity occurring in what appears to be certain grain boundaries of the surface. Conduction through grain boundaries, as shown in this CSAFM image, fits the form of ion conduction through the interface proposed by Peled et al. [10].

Figure 2.4 is a lithium surface after exposure for three days to the PEO/LiCF<sub>3</sub>SO<sub>3</sub> electrolyte not having the protective monolayers. The grains appear to have enlarged to an average size of 250 nm. In addition, most regions of the surface have developed relatively large crystal-like structures of 600-700 nm in dimension. As discussed previously and shown in Figure 2.2, lithium surfaces that have been exposed to the PEO/LiCF<sub>3</sub>SO<sub>3</sub> electrolyte form passivation layers. What is seen in the CSAFM image must be such a passivation layer. CSAFM images were obtained for this passivated lithium surface and, even at potentials as high as -5 volts, no appreciable current conduction could be found, resulting in a featureless CSAFM image (not shown). This is in contrast to Figure 2.3c of the non-passivated surface where current can be detected readily even at the bias potential of only -0.5 volts.

More information concerning the actual species present at the lithium/polymer electrolyte interface was obtained by ATR-FTIR spectroscopy. Spectra collected at the interface of a lithium/electrolyte interface undergoing passivation is shown in Figures 2.5 and 2.6. Figure 2.5 shows the CH stretching region showing the change in these vibrational modes as a function of time. The interesting feature in these spectra is the emergence of a mode at 2962 cm<sup>-1</sup>, which is the frequency of the CH stretch of a methyl, CH<sub>3</sub>, group. This mode continues to increase in intensity until it appears to reach equilibrium by day 2, as the spectra for day 5 is virtually identical. Figure 2.6 is a much wider region of the ATR-FTIR spectrum also having interesting features. In order to gain an appreciation for the speed at which changes are occurring at the lithium interface, a PEO-triflate film not in contact with lithium is shown in the Figure (bottom spectrum). The spectrum of a PEO-triflate film after 15 minutes contact with lithium is also shown in Figure 2.6 (middle spectrum). Even after this short time, changes in the spectrum occur. Peaks at 1260 cm<sup>-1</sup>, 1160 cm<sup>-1</sup> and 1045 cm<sup>-1</sup> are observed. After 21 hours of contact with lithium (top spectrum) these modes have continued to grow and modes at 1010 cm<sup>-1</sup> and

790  $\text{cm}^{-1}$  can now be seen. Spectra collected for longer time periods show no new vibrational modes and the modes present simply increase slightly in intensity until equilibrium is reached by the second day of lithium contact. ATR-FTIR spectra of the lithium/polymer interface protected by the self-assembled monolayers show virtually no formation of the vibrational modes described above, once again indicating passivation protection.

Interpretation of complicated vibrational spectra can be challenging. However, well-known peak assignments and work conducted by other researchers can be of help. The simultaneous occurrence of the relatively strong modes at 1260 and 1045  $\text{cm}^{-1}$  is commonly associated with =C-O-C- group [11] while the mode at 1160  $\text{cm}^{-1}$  is the correct frequency for the C-F bonds in  $\text{HCF}_3$  [11]. This could be associated with Vincent's proposed reaction of lithium triflate with lithium metal [3]



Vincent proposed that the  $\text{CF}_3$  radical would extract a hydrogen atom from the PEO polymer chain forming  $\text{HCF}_3$  and perhaps result in the breaking of the polymer chain. The =C-O-C- group could result from this main chain breaking. The occurrence of these modes after only 15 minutes of contact with lithium indicates that this could be one of the first reactions to occur. Vibrational modes seen after 21 hours' contact with lithium can be assigned to different chemical species. These modes (1010 and 790  $\text{cm}^{-1}$ ) have frequencies similar to Li-O-R and Li-O-R-O-Li compounds formed when lithium metal was exposed to glyme compounds [4,5]. For instance a mode in the range of 1100 -1000  $\text{cm}^{-1}$  has been associated with the C-O stretch of lithium alkyoxides and the strong mode at 790  $\text{cm}^{-1}$  is reasonably close to a mode of similar frequency (780  $\text{cm}^{-1}$ ) and intensity observed in the IR spectrum of lithium ethoxide [4]. The appearance and increasing intensity of the 2962  $\text{cm}^{-1}$  peak must arise from polymer backbone breaking and an accompanying formation of  $\text{CH}_3$  end groups. The formation of  $\text{CH}_3$  by chain scission could be due to either the  $\text{CF}_3$  radical attack on the chain or the breaking of the -C-O- bond to form the Li-O-R compounds. Hydrogen would be available for this reaction from the formation of double bonds or from the inevitable presence of very small amounts of water. However, since this peak is not seen after 15 minutes' contact with the lithium but after longer time periods (see Figure 2.6), it may mainly result from the formation of the Li-O-R compounds. Whatever the source of the methyl groups, they must result from the  $\text{CH}_3$  hydrogen stretch of a  $\text{CH}_3\text{-CH}_2\text{-}$  end group, since  $\text{CH}_3$  stretching modes from  $\text{CH}_3\text{-O-R}$  or  $\text{CH}_3\text{-O-Li}$  occur 20-30  $\text{cm}^{-1}$  lower in frequency [4].

## 2.4. Conclusions

The passivation layer formed when lithium metal is in contact with PEO-triflate electrolyte has been investigated. Lithium surface films composed of grains and crystalline regions can be observed by AFM and CSAFM. AFM and CSAFM images indicate that these films have low conductivities compared to lithium surfaces where passivation has been inhibited by the adsorption of self-assembled monolayers. ATR-FTIR studies of the lithium/polymer interface indicate that one of the first reactions in the

passivation process at the lithium/polymer electrolyte interface is the formation of the  $\text{CF}_3$  radical, which quickly extracts a hydrogen atom from the polymer backbone. Somewhat later in the reaction scheme, lithium also begins to break the polymer chain at the C-O bond forming Li-O-R type compounds. Interestingly, it appears that many of the end groups resulting from these polymer chain-breaking reactions are of the form  $\text{CH}_3\text{-CH}_2\text{-}$ . This is one of the few characterizations conducted on the lithium electrode/polymer electrolyte interface in terms of the actual chemical species present. This study provides the background necessary to understand how adsorbed molecular layers inhibit passivation.

## 2.5. References

1. D. Fateaux, *J. Electrochem. Soc.* **135**, 2231(1998).
2. P. G. Bruce and F. Krok, *Solid State Ionics*, **36**, 171 (1989).
3. C. A. Vincent, *Prog. Solid State Chem.* **17**, 145 (1987).
4. D. Aurbach and E. Granot, *Electrochimica Acta*, **42**, No.4. 697 (1997).
5. D. Aurbach, M.L. Daroux, P. Faguy and E.B. Yeager, *J. Electrochem. Soc.*, **135**, 1863 (1988).
6. A. Lisowska-Oleksiak, *Solid State Ionics* **119**, 205 (1999).
7. I. Rey, J.C. Lassegues, P. Baudry and H. Majastre, *Electrochimica Acta*, **43**, No. 10-11, 1539 (1998).
8. J.B. Kerr, J. Hou, S. Wang, S.E. Sloop, O. Buriez, Y.B. Han, *Polymeric Materials Science and Engineering proceedings*, March 21-25, 1999
9. K. Morigaki and A. Ohta, *J. Power Sources*, **76**, 159 (1998).
10. E. Peled, D. Golodnitsky, G. Ardel and V. Eshkenazy, *Electrochimica Acta*, **40**, No. 13, 2197 (1995).
11. A. J. Gordon and R.A. Ford, *The chemist's companion*, Wiley Interscience publication

## 2.6. Figures

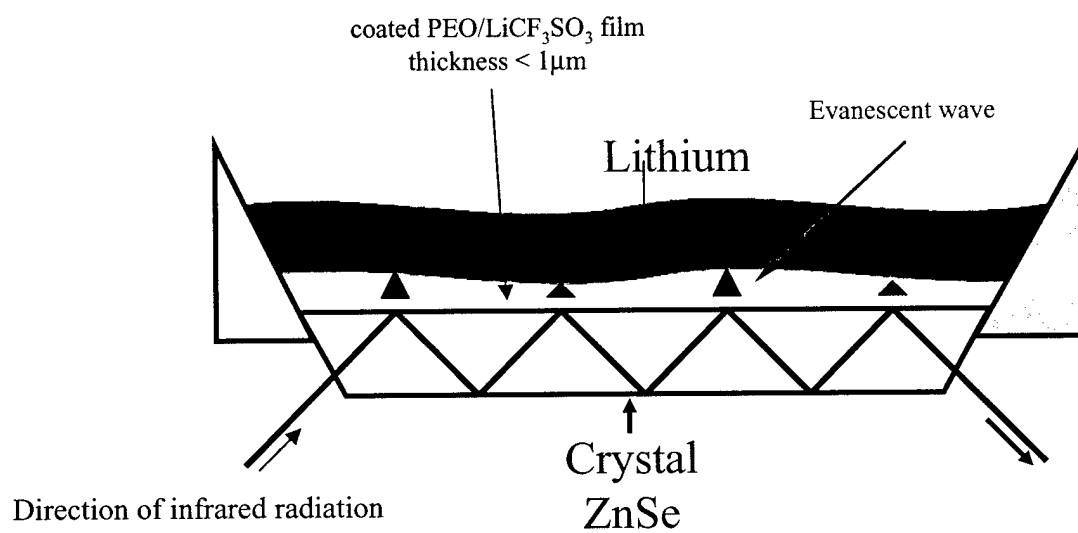


Figure 2.1

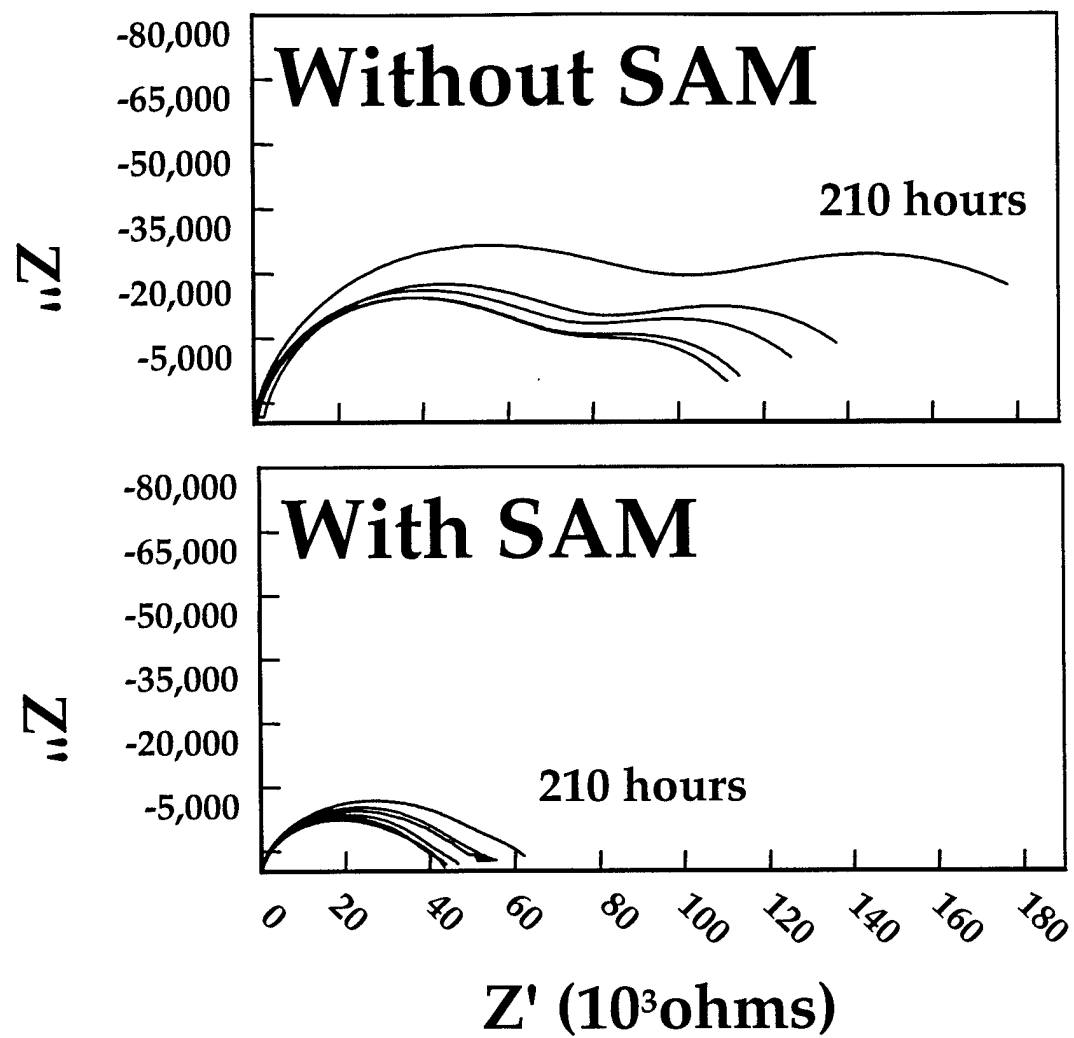


Figure 2.2

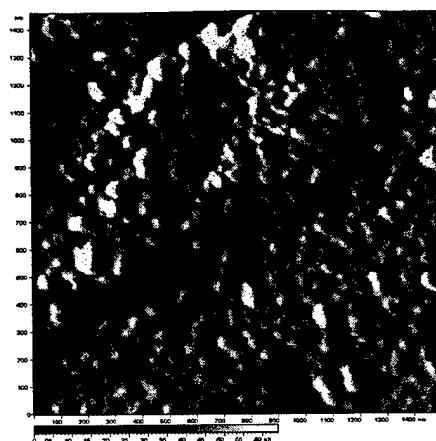


Figure 2.3a

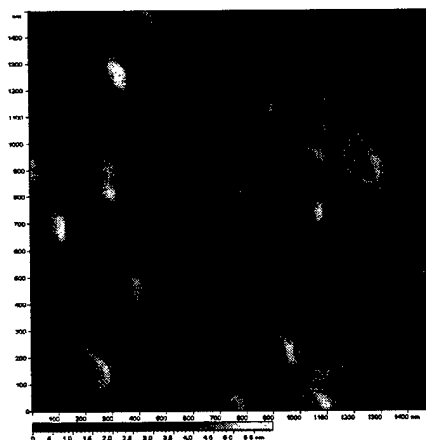


Figure 2.3b

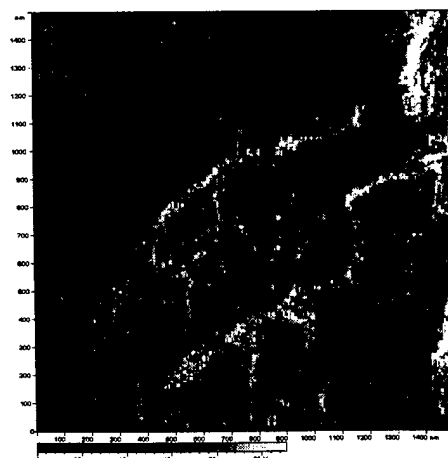


Figure 2.3c





Figure 2.4

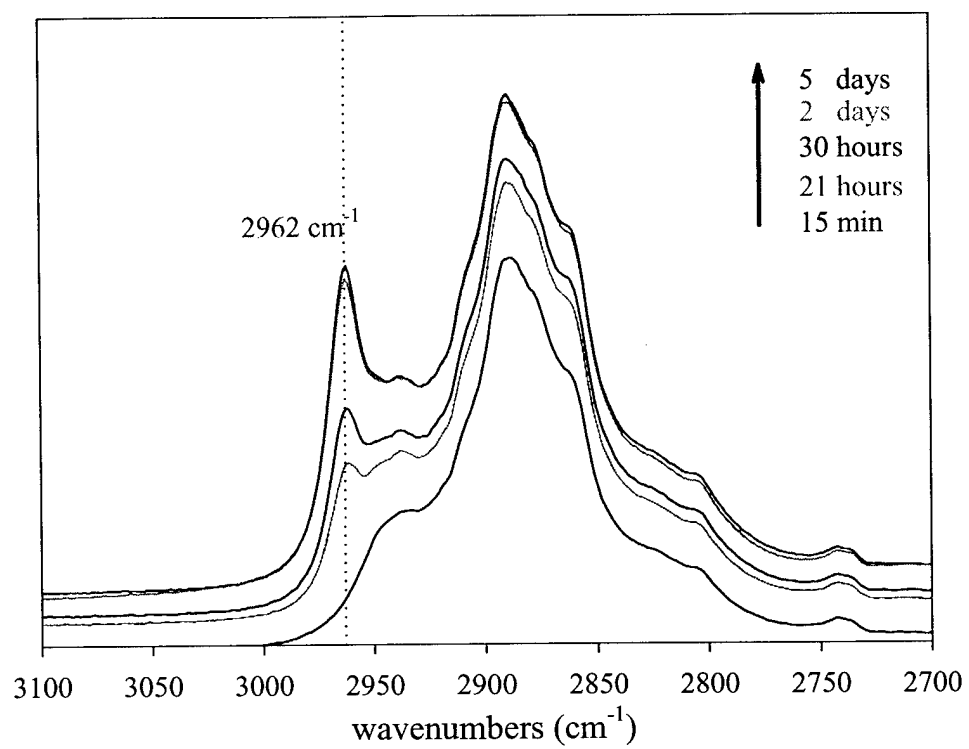


Figure 2.5

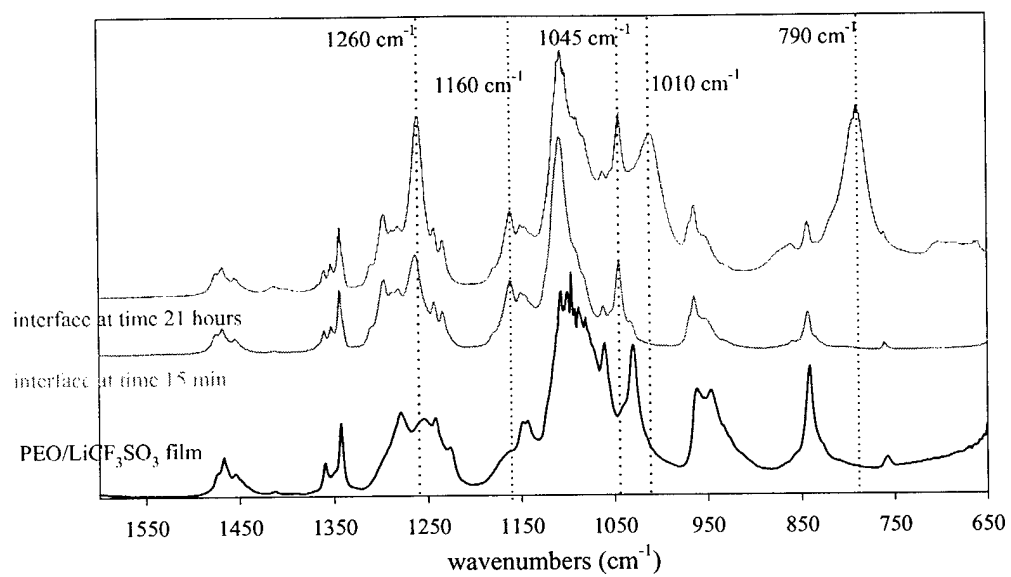


Figure 2.6

## Chapter 3. Further Investigations of Self-Assembled Monolayers Ability to Prevent Passivation

### 3.1. Introduction

Recent studies conducted in our laboratory [1-4] and discussed in Chapters 1 and 2 of this report have shown that self-assembled molecular layers placed on the polymer electrolyte surface can stabilize the interface under open circuit conditions. Our ATR-FTIR, critical surface tension, and atomic force microscope, AFM, studies have shown that molecules of the form  $\text{H}-(\text{CH}_2)_m-(\text{CH}_2-\text{CH}_2-\text{O})_n-\text{H}$  adsorb on poly(ethylene oxide), PEO, electrolyte surfaces in the manner shown in Figure 3.1. The poly(ethylene oxide)-like portion of these molecules preferentially orient to adsorb onto the poly(ethylene oxide) electrolyte film. This leaves the  $\text{CH}_2$  segment of the molecule to self-assemble into an ordered layer just above the electrolyte surface. The hydrocarbon layer, which now comes in direct contact with the lithium instead of the polymer electrolyte, is not reactive with the metal and stabilizes the interface.

The solid electrolyte interphase (SEI) is a well-established concept in lithium batteries [5,6] and we feel that this SAM layer forms a new type of SEI that helps to stabilize the interface. One problem that might be expected with this hydrocarbon SEI is that the hydrocarbon layer would act as an insulator or a barrier to ion conduction through the interface between the electrode and the electrolyte. However, we have measured the movement of ions through this hydrocarbon layer and have found it to be only slightly lowered, most likely due to the ions' ability to move through defects in the layer [2]. Interestingly, in studies conducted at  $50^\circ\text{C}$ , we have consistently measured apparent bulk ion conductivities of the polymer films with SAMs that are slightly higher than polymer electrolyte films without the SAM. This appears to be due to better contact between the lithium metal and the polymer electrolyte film as a result of a smoother surface on the molecular level. We have found that the presence of SAMs at the lithium/polymer electrolyte interface has stabilized the interface under open circuit conditions for periods of time exceeding two weeks [1,2].

Important questions that remained to be answered were how these SAM layers would hold up under temperatures higher than  $50^\circ\text{C}$  and under typical battery cycling conditions. This is the subject of the work presented below.

### 3.2. Experimental

Symmetric lithium cells ( $\text{Li}/\text{polymer electrolyte}/\text{Li}$ ) were made from two lithium electrodes each having surface areas of  $1.60\text{ cm}^2$ . The lithium ribbon used for this was 0.0125 inch thick and was obtained from Aldrich Chemicals. The electrolyte films were made from PEO (MW = 900,000) and lithium trifluoromethanesulfonate (triflate) salt, both obtained from Aldrich, and the ratio of ether oxygens to lithium ions in the polymer was 15:1. The complete procedure for making and storing the films and cells, which was done either under nitrogen or argon, can be found elsewhere [1,2]. The thickness of the films ranged from 100 to 130  $\mu\text{m}$ . PEO electrolytes with self-assembled molecular layers adsorbed on the surface were prepared as described in Chapter 1. Semicrystalline wax

from Petrolite Specialty Polymers, described as  $\text{H}-(\text{CH}_2)_{32}-(\text{CH}_2-\text{CH}_2-\text{O})_{10}-\text{H}$ , was used to form the self-assembled molecular layers, as depicted in Figure 3.1. Nickel foil (0.125mm thick) from Aldrich chemicals was used to make the current collectors, and the cells were assembled as Ni/Li/Polymer Electrolyte/Li/Ni in a glove box under argon purge and placed in a sample holder. The sample holder was then placed in a glass tube fitted with a rubber sealing stopper, and the glass tube was evacuated and placed in an oil bath at a temperature of 75°C controlled to  $\pm 0.01^\circ\text{C}$ . While some cells were allowed to stay under open circuit conditions for extended periods of time, others were cycled using a MACCOR model 2300 battery test system. Each cycle consisted of a charge step of  $150 \mu\text{A}/\text{cm}^2$  for 30 minutes followed by a discharge at the same current density for another 30 minutes. After 20 such cycles, impedance measurements were made using a Hewlett-Packard 4914-A a.c. impedance/gain phase analyzer. The impedance data were obtained in a 100Hz-40MHz frequency range.

Analysis of the impedance data was done using ZView (Scribner Associates) electrochemical impedance modeling software. An equivalent circuit analysis of the type proposed by Munichandraiah, Scanlon, and Marsh [7], for lithium metal/polymer electrolyte systems, seemed to describe the impedance data well. For these studies done at 75°C the polymer electrolyte appears to act as a pure resistor, while a high frequency semicircle, due to the interface, is represented by a resistance  $R_p$  in parallel with a constant phase element. A second low frequency semicircle is represented by a resistance  $R_{ct}$ , also in parallel with a constant phase element.

Cyclic voltammetry work was done using an EG&G Princeton Applied Research potentiostat/galvanostat Model 273. All cyclic voltammetry tests were done at a scan rate of 5 mV/sec.

### 3.3. Results and Discussion

Figure 3.2 shows the Nyquist plot for a symmetric lithium cell under open circuit conditions kept in an oil bath at 75° C for approximately six days. The high frequency semicircle corresponds to the interfacial resistance due to passivation; the low frequency semicircle corresponds to the resistance to charge transfer; and the left  $Z'$  axis intercept of the high frequency semicircle corresponds to the bulk electrolyte resistance. It is evident from the data that the high frequency semicircle grows with time due to the growing passivation layer. Growth of the low frequency semicircle associated with charge transfer indicates that charge transfer resistance also increases with time. Since the products of the passivation reaction are known to be poor conductors, it is reasonable that charge transfer becomes more difficult as the passivation layer builds on the electrode surface. The rate of growth of the passivation layer eventually slows and, after some time, appears to stop. The charge transfer resistance also remains constant once the passivation layer stops growing. Such complex behavior is typical of the lithium/polymer electrolyte interface and has been seen by other researchers [8].

A much different behavior is observed for lithium symmetric cells with SAMs at the interface. Nyquist plots for this system are shown in Figure 3.3. Here the high frequency semicircle does not grow with time, which indicates that the growth of the passivation layer is inhibited and/or stabilized resulting in little change in the interfacial

resistance. However, the charge transfer resistance increases with time and in this case is higher compared to the data where there are no SAMs at the interface. The higher charge transfer resistance can be attributed to the blocking properties of the SAMs since SAMs are known to block electrochemical reactions and slow the kinetics of this process [9-14]. The increase in the charge transfer resistance could be due to better packing of the SAM tails with time resulting in increased blocking behavior.

The behavior described above can be seen more quantitatively by looking at resistance versus time plots. Figure 3.4 is a plot of the interfacial resistance as a function of time for the impedance data shown in Figures 3.2 and 3.3. The passivation resistance increases for the cell without SAMs at the interface and is initially quite large. The rate of increase slows, but nevertheless continues to increase. At similar times, the cell with self-assembled molecular layers at the interface shows little or no increase in the interfacial resistance, indicating that the interface has been stabilized. It is important to note that at all times the interfacial resistance is higher for the cell without SAMs at the interface.

The charge transfer resistances for the impedance data shown in Figures 3.2 and 3.3 is shown in Figure 3.5. At all times, the charge transfer resistance for the cell with SAMs at the interface is higher than the system without these monolayers, most likely because of the blocking properties of the SAM. For the case of no SAMs at the interface, the change in the charge transfer resistance closely mirrors the behavior of the growth of the passivation layer resistance at the interface (see Figure 3.4). During the initial rapid growth of the passivation layer, the charge transfer resistance also increases dramatically. At later times, there is only a slight increase in the passivation resistance and the charge transfer resistance behaves similarly. In fact, it slightly decreases with time. It is known that the passivation layers, under cycling, change structure and become more compact as time progresses, sometimes eventually forming a more stable interface [15]. This appears to be what is happening here.

It is clear from the above results that SAMs, when present at the electrode/electrolyte interface, are effective in inhibiting passivation of the electrode under open circuit conditions. Our past work, using ATR-FTIR spectroscopy to investigate the lithium/polymer interface, has indicated that interface stabilization under open circuit conditions may primarily be due to the hydrocarbon tails of the SAM, thereby keeping the reactive lithium metal away from the polymer electrolyte surface [3]. This prevents lithium from having chain scission reactions with the PEO backbone and reactions with the lithium salt anion that destabilize the interface. However, it is important to evaluate the molecular layer's effectiveness at conditions other than an open circuit. Typical battery cycling test would place the SAMs under the electrochemical stress that they must handle in battery systems.

In order to investigate the effects of cycling, a.c. impedance analysis was done for cells that were electrochemically cycled. The cells used for these studies were, as before, lithium symmetric cells maintained at a temperature of 75° C. As mentioned earlier, each cycle consisted of a charge step followed by a discharge step. Both steps were carried out at a constant current of 150  $\mu\text{A}/\text{cm}^2$  for 30 minutes each. AC. impedance measurements were done after every 20 cycles.

The variation of the interfacial resistance over approximately four days for cells with and without SAMs at the interface is shown in Figure 3.6. It is clear that the interfacial resistance for both of the cells increases with time under cycling conditions. However, the interfacial resistance is always less for the cell with SAMs at the interface. This indicates that SAMs are useful in stabilizing passivation under cycling conditions just as they were under open circuit conditions, though their stabilizing properties are weakened during the cycling process. The variation of charge transfer resistance with time is shown in Figure 3.7. Similar to the open circuit tests, the charge transfer resistance is higher for the cells with SAMs at the interface, again because of the blocking properties of SAMs. For both systems, there is virtually no change in the resistance with time.

To further study the stability of the SAM layer, a cell with SAMs at the interface was kept under open circuit conditions for 150 hours. Periodically, during this time a.c. impedance data were collected. When the elapsed time reached 150 hours, cyclic voltammetry was used to take the lithium in the cell through a plating-stripping cycle. Starting at 200 hours, a.c. impedance data were collected again. The interfacial and charge transfer resistance data for this study are shown in Figures 3.8 and 3.9 respectively. For the sake of comparison, the results of a cell with no SAMs at the interface, kept under similar open circuit conditions and having gone through the same plating-stripping cycle, are included in these Figures.

The data in Figure 3.8 indicates that after the oxidation reduction cycling there is a sudden increase in the interfacial resistance for the interface with the SAM though the resistance does not become higher than that for a cell with no SAMs at the interface. Driving the metal through a lithium plating stripping cycle appears to degrade the SAM somewhat. The plot of charge transfer resistance in Figure 3.9 shows the opposite behavior. It can be seen that this resistance drops for the cell with SAMs at the interface after cycling. Once again this can be attributed to the degradation of the SAM. With this degradation, the charge transfer process is not slowed as much as it was when the SAM was in its more pristine, non-degraded state. The chemical mechanism associated with this degradation process will be the object of future research in our laboratory.

### 3.4. CONCLUSIONS

From the discussion above, it is clear that SAMs used in this study, to temperatures at least as high as 75°C, are good at stabilizing the lithium metal/polymer electrolyte interface under open circuit conditions for periods of six days and longer. Our past work [3] has indicated that interface stabilization may primarily be due to the hydrocarbon tails of the SAM keeping the reactive lithium metal away from the polymer electrolyte surface where reactions with the PEO backbone and reactions with the lithium salt anion can easily occur, forming a passivation layer that is highly resistant to ion flow.

With cycling, there is some apparent degradation of the SAM layers which decreases the effectiveness of SAMs to stabilize the interface under extended time tests. This is made evident by the increase in passivation resistance. However, even under cycling conditions for time periods as long as nine days, the passivation resistance for

interfaces where the SAMs are present, is always at lower than interfaces that are not protected by the SAMs.

It is obvious from the data presented here that there are two areas that must be investigated if SAM technology is to reach its full potential in battery technology. First, the increase in the charge transfer resistance caused by the blocking nature of the SAMs must be addressed. One way to approach this is to shorten the length of the hydrocarbon tails of the molecules used to make the SAMs, which will presumably make charge transfer easier. However, a trade-off between the ability of the SAM to stabilize the interface and a decrease in charge transfer resistance will probably result. Research is being conducted in our laboratory where interface stabilization and ease of charge transfer are being maximized by changing the chemical make-up of the molecules used to make the SAM. The second area of concern is the stability of the SAM under cycling conditions. Likewise this factor may also be able to be addressed by the chemistry of the molecules used to make the SAM. Previous work in our laboratory has shown that molecules having groups such as poly(dimethyl siloxanes) and branched hydrocarbon chains can be adsorbed onto the polymer surface [8]. While these molecules when adsorbed on the surface of the polymer electrolyte may not form the ordered, self-assembled structures like those studied here, they do form self-assembled molecular "brush" layers that are nevertheless densely backed enough to stabilize the lithium/electrolyte interface. Thus, because of the numerous chemistries that can be tried, SAMs of appropriate chemical composition may be found that will better withstand battery cycling. Changing the chemical make-up of the SAMs seems to presents many interesting opportunities to maximize their performance and to better understand their mechanism of stabilization.

This work has shown the potential for molecular self-assembly to stabilize the interfaces importance to lithium/polymer electrolyte systems. It seems reasonable to assume that this technology could also be used to stabilize the cathode/electrolyte interface. It also should be amenable to plasticized and gelled polymer electrolyte systems, perhaps eventually making them more suited for use with solid lithium electrodes. This technique appears to be one potential example where nanotechnology is able to live up to its promised significance and solve macroscopic problems of technical importance.

### 3.5. References

1. R. N. Mason, M. Smith, T. Andrews, and D. Teeters, *Solid State Ionics*, **118**, 129 (1999).
2. M. Le Granvalet-Mancini, L. Honeycutt, D. Teeters, *Electrochimica Acta*, **45**, 1491 (2000).
3. M. Le Granvalet-Mancini, T. Hanrath, and D. Teeters, *Solid State Ionics*, **135/1-4**, 283 (2000).
4. M. Le Granvalet-Mancinia and D. Teeters, *Journal of Power Sources*, **97-98**, 624 (2001).



5. E. Peled, in *Lithium Batteries*, J. P. Gabano, Editor, p. 43-72, Accademic Press (1983).
6. E. Peled, J. Electrochem. Soc., **126**, 2047 (1979).
7. N. Munichandraiah, L. G. Scanlon, and R. A. Marsh, J. Power Sources, **72**, 203 (1998)
8. D. Fauteux, Solid State Ionics, **17**, 133 (1985).
9. H. O. Finklea, D. A. Snider and J. Fedyk, Langmuir, **9**, 3660 (1993).
10. K. Tokuda, T. Gueshi, and H. Matsuda, J. Electroanal. Chem., **102**, 41 (1979).
11. H. Gerischer, Z. Phys. Che., **198**, 286 (1951).
12. A. J. Bard and L. R. Faulkner, in *Electrochemical Methods: Fundamentals and Applications*, John Wiley & Sons, New York (1980).
13. D. E. Smith, in *Electroanalytical Chemistry*, A. J. Bard, Editor, p. 1-155, Marcel Dekker, New York (1966).
14. M. Sluyters-Rehbach and J. H. Sluyters, in *Electroanalytical Chemistry*, A. J. Bard, Editor, p. 1-128, Marcel Dekker, New York (1970).
15. C. Julien and G. Nazri, in *Solid State Batteries: Materials Design and Optimization*, C. Julien and G. A. Nazri, Editors, p. 12, Kluwer Academic Publishers, Boston (1994).

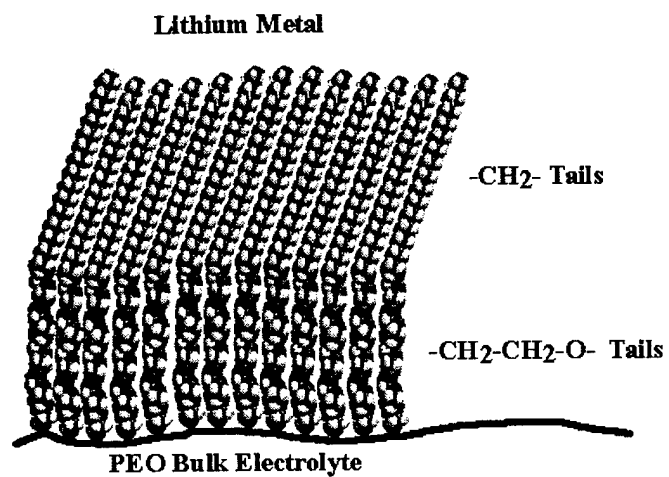


Figure 4.1. Illustration of the SAM on the polymer electrolyte surface. The  $(\text{CH}_2\text{-CH}_2\text{-O})_n$  portion of the SAM molecules adsorbs on the polymer electrolyte surface. The self-assembled  $(\text{CH}_2)_m$  part of the SAM molecule comes in contact with the lithium metal when cells are formed.

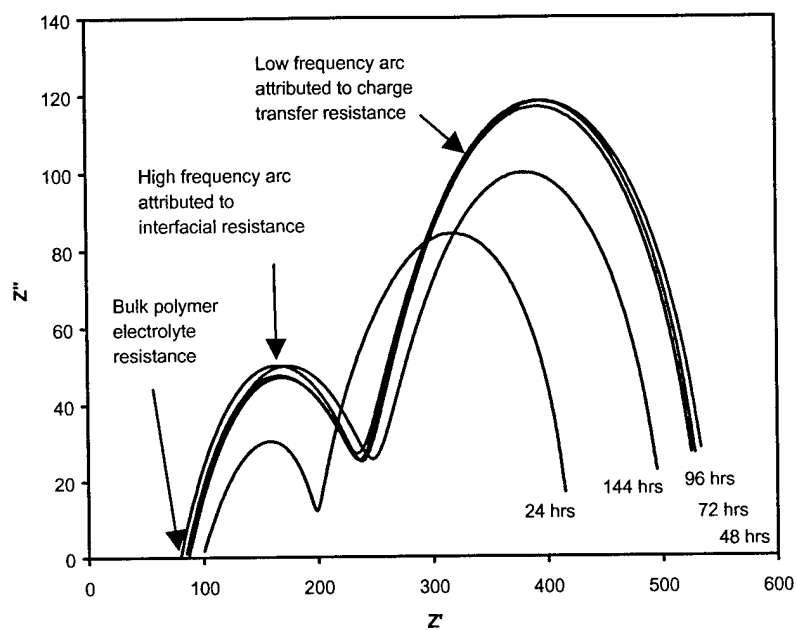


Figure 4.2. A.C. impedance data for lithium/PEO-lithium triflate/lithium cell @ 75°C without SAM stabilization. Cell was kept under open circuit conditions.

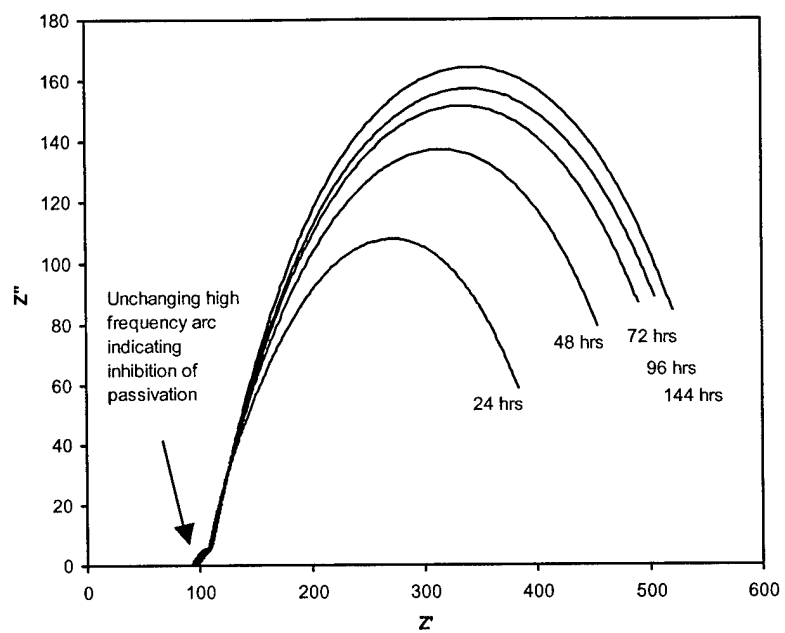


Figure 4.3. A.C. impedance data for lithium/PEO-lithium triflate/lithium cell@ 75°C with SAM stabilization. Cell was kept under open circuit conditions.

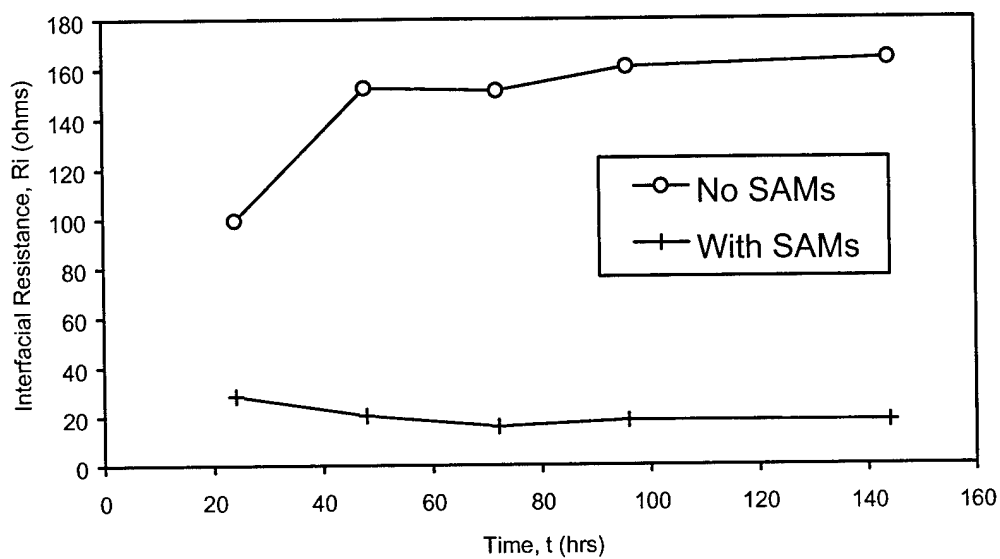


Figure 4.4. Interfacial resistance as a function of time for lithium/PEO-lithium triflate/lithium cells @ 75°C. Cells were kept under open circuit conditions. Data are shown for cells with and without SAM stabilization.

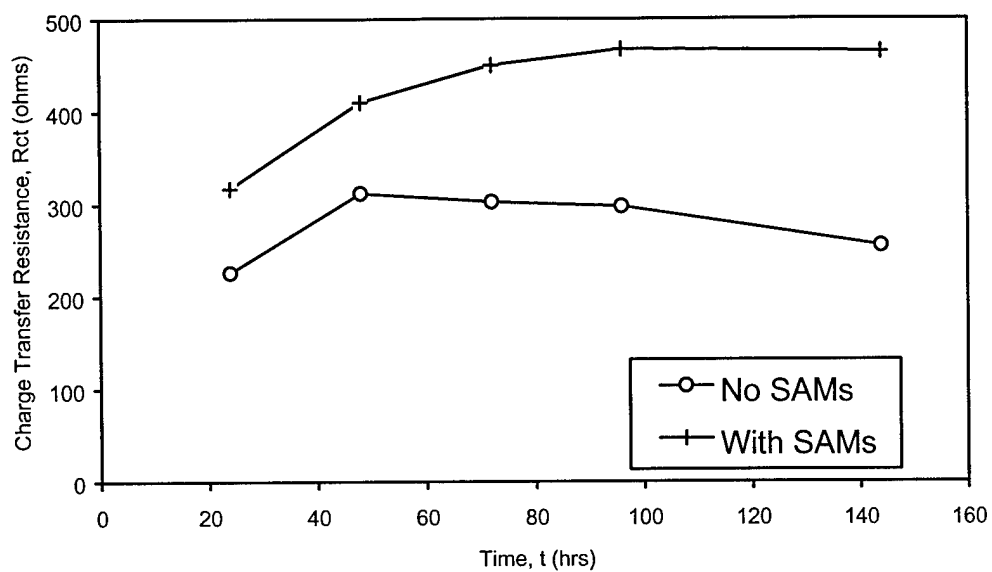


Figure 4.5. Charge transfer resistance as a function of time for lithium/PEO-lithium triflate/lithium cells @ 75°C. Cells were kept under open circuit conditions. Data are shown for cells with and without SAM stabilization.

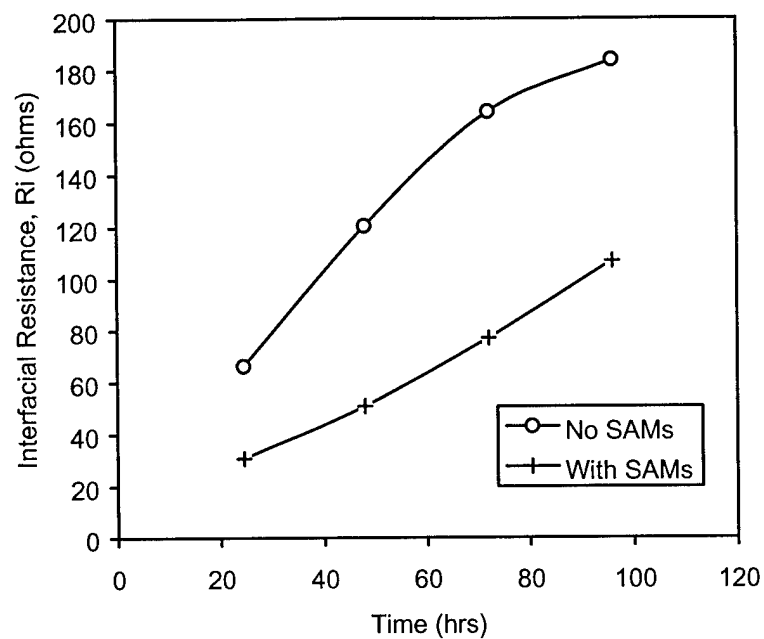


Figure 4.6. Interfacial resistance as a function of time for lithium/PEO-lithium triflate/lithium cells @ 75°C. The cells were continuously cycled with a 30 minute charge/30 minute discharge cycle at a constant current of  $150 \mu\text{A}/\text{cm}^2$ . Data are shown for cells with and without SAM stabilization.

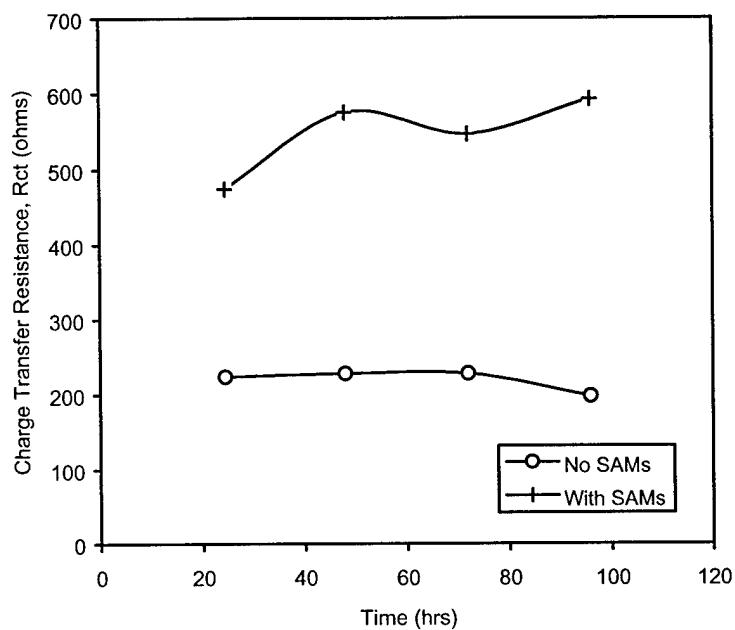


Figure 4.7. Charge transfer resistance as a function of time for lithium/PEO-lithium triflate/lithium cells @ 75°C. The cells were continuously cycled with a 30 minute charge/30 minute discharge cycle at a constant current of  $150 \mu\text{A}/\text{cm}^2$ . Data are shown for cells with and without SAM stabilization.



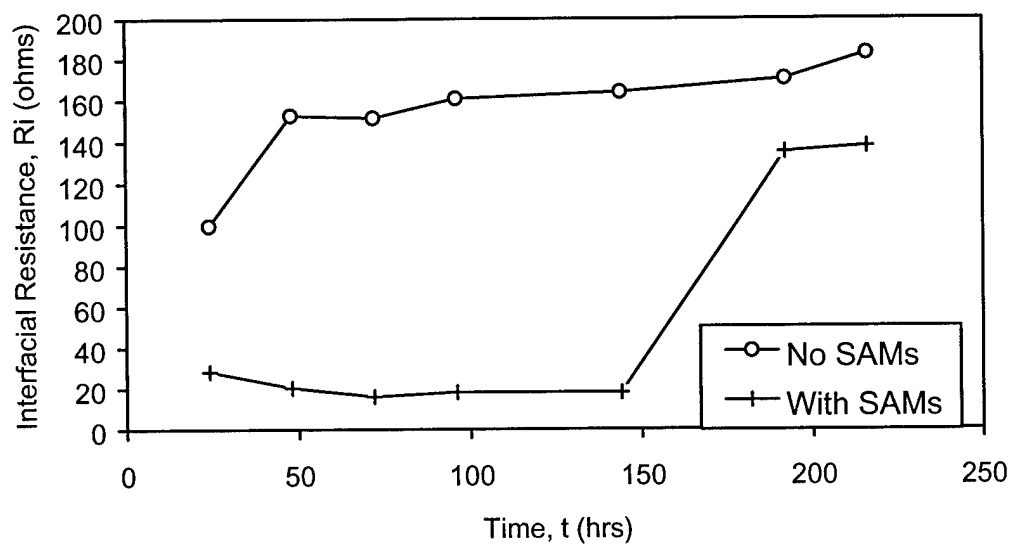


Figure 4.8. Interfacial resistance as a function of time for lithium/PEO-lithium triflate/lithium cells @ 75°C. Cells were kept under open circuit conditions for approximately 150 hours, then a lithium plating-stripping cycle was performed by using cyclic voltammetry. Cells were returned to open circuit conditions for the rest of the experiment. Data are shown for cells with and without SAM stabilization.

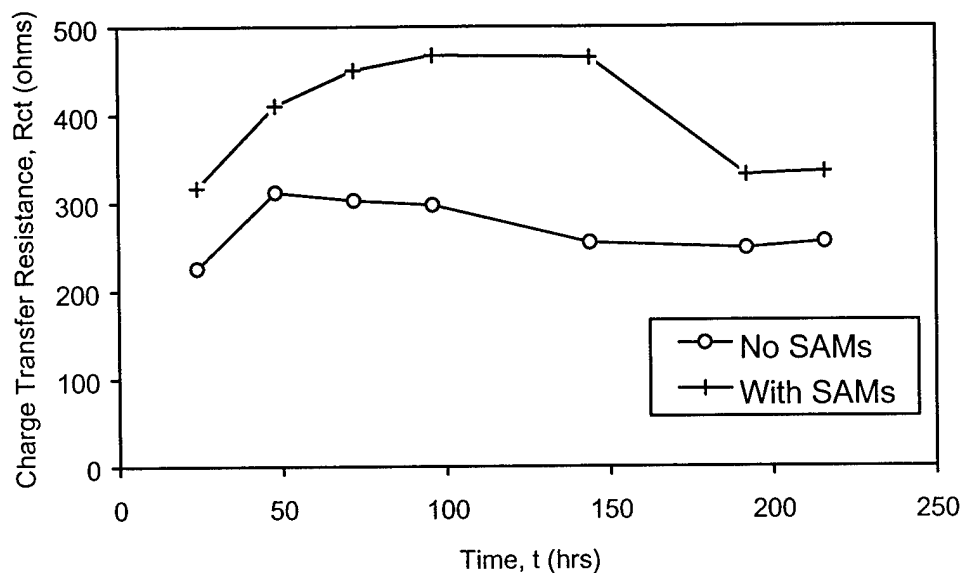


Figure 4.9. Charge transfer resistance as a function of time for lithium/PEO-lithium triflate/lithium cells @ 75°C. Cells were kept under open circuit conditions for approximately 150 hours, then a lithium plating/stripping cycle was performed. Cells were returned to open circuit conditions for the rest of the experiment. Data are shown for cells with and without SAM stabilization.

## Chapter 4. The Effects of Chemical Composition of Adsorbed Molecular Layers on Lithium Electrode/Polymer Electrolyte Interface Stabilization

### 4.1. Introduction

Recent studies conducted in our laboratory [1,2] have shown that self-assembled molecular layers placed on the polymer surface can offer protection from passivation and stabilize the interface. AC impedance spectroscopy has shown that molecules of the form  $\text{H}-(\text{CH}_2)_m-(\text{CH}_2-\text{CH}_2-\text{O})_n-\text{H}$  adsorbed on PEO electrolyte surfaces and that they stabilize the lithium/polymer electrolyte interface in lithium symmetric cells stored under an open circuit potential [1,2]. It appears that the poly(ethylene oxide)-like portion of these molecules preferentially orient to absorb onto the poly(ethylene oxide) electrolyte film. This leaves the  $\text{CH}_2$  segment of the molecule to self-assemble into an ordered layer just above the electrolyte surface. Studies show that this hydrocarbon layer, which now comes in contact with the lithium instead of the polymer electrolyte, is not reactive with the metal and stabilizes the interface by forming a new type of solid electrolyte interphase (SEI) [2]. Movement of ions through this hydrocarbon layer is only slightly lowered, most likely due to the ions' ability to move through defects in the layer [2].

This section of the report is concerned with how changing the chemistry of the adsorbed molecules affects the ability of the molecules to adsorb and the ability to stabilize the lithium/polymer electrolyte interface.

### 4.2. EXPERIMENTAL

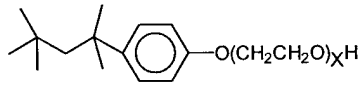
Previous work used semicrystalline waxes having the general form  $\text{H}-(\text{CH}_2)_m-(\text{CH}_2-\text{CH}_2-\text{O})_n-\text{H}$  as the molecules for adsorption on the polymer electrolyte surface [19]. For this work other molecules that might adsorb on the polymer surface and provide interface stabilization were used. A long, straight-chain alcohol and a long, straight-chain carboxylic acid from Petrolite Specialty Polymers, two siloxane surfactants from Dow Corning, and the surfactant Triton X100 from Acros Chemicals were studied. Formation of adsorbed layers was accomplished via adsorption from a hexane solution, and the complete procedure for film preparation and formation of the self-assembled molecular layers on the film has been describe previously [1,2]. Surface infrared spectra, using the ATR technique, were collected on a Nicolet 510P fourier transform infrared spectrometer with a DTGS detector at  $1\text{ cm}^{-1}$  spectral resolution. The average depth of penetration of the infrared radiation into the surface can be calculated [2] and was found to be approximately  $1.0\text{ }\mu\text{m}$ . An HP 4194-A ac impedance/gain phase analyzer was used to investigate the electrochemistry of symmetric lithium cells. This was done over a range of 40MHz to 10KHz. Test cells for impedance analysis were assembled in a glove box under argon purge and ac impedance tests were done at  $50^\circ\text{C}$  under vacuum.

### 4.3. RESULTS AND DISCUSSION

The molecules used in adsorption studies in this investigation and, for comparison, those used in previous adsorption work are given in Table 1. The presence of

the adsorbed molecular layers was determined by ATR-FTIR spectroscopy as reported previously [1,2]. All molecules investigated in this work adsorbed on the PEO polymer electrolyte surface.

**Table 1**

Chemical Formula	Ability to Stabilize Lithium/Polymer Interface
$\text{H}(\text{CH}_2)_{32}(\text{CH}_2\text{CH}_2\text{O})_3\text{H}$	Yes <sup>a</sup>
$\text{H}(\text{CH}_2)_{32}(\text{CH}_2\text{CH}_2\text{O})_{10}\text{H}$	Yes <sup>a</sup>
$\text{H}(\text{CH}_2)_{40}(\text{CH}_2\text{CH}_2\text{O})_3\text{H}$	Yes <sup>a</sup>
$\text{H}(\text{CH}_2)_{40}(\text{CH}_2\text{CH}_2\text{O})_{13}\text{H}$	Yes <sup>a</sup>
$\text{H}(\text{CH}_2)_{50}\text{OH}$	No
$\text{H}(\text{CH}_2)_{77}-\overset{\text{O}}{\underset{\text{  }}{\text{C}}}-\text{OH}$	No
$\text{HO}-(\text{CH}_2\text{CH}_2\text{O})_{12}-\left(\overset{\text{CH}_3}{\underset{\text{CH}_3}{\text{Si}}}-\text{O}\right)_{15}-(\text{CH}_2\text{CH}_2\text{O})_{12}-\text{H}$	Yes
$\text{CH}_3-\overset{\text{CH}_3}{\underset{\text{CH}_3}{\text{Si}}}-\text{O}-\left(\overset{\text{CH}_3}{\underset{\text{CH}_3}{\text{Si}}}-\text{O}\right)_{8.7}-\left(\overset{\text{CH}_3}{\underset{\text{C}_3\text{H}_6\text{O}}{\text{Si}}}-\text{O}\right)_{3.7}-\text{CH}_3$ $\text{C}_3\text{H}_6\text{O}-(\text{CH}_2\text{CH}_2\text{O})_{12}-\text{H}$	Yes
 where X = 9-10	Yes

<sup>a</sup>Previous work Chapter 1 and reference 2.

AC impedance data for lithium symmetric cells were collected at various times to a maximum time of approximately 160 hours for PEO electrolyte films and PEO electrolyte films with the molecules listed in Table 1 adsorbed on the surface. Nyquist plots for PEO films with the  $\text{H}-(\text{CH}_2)_{50}-\text{OH}$  or  $\text{H}-(\text{CH}_2)_{77}-\text{COOH}$  molecules adsorbed onto the surface show two overlapping semicircles present in the lithium symmetric cells at open circuit voltage. The capacitance of these semicircles was estimated by knowing that the maximum of each semicircle should obey the relation  $\omega\text{RC} = 1$ . The first semicircle has a capacitance in the range of pFs usually associated with the bulk response while the second has a value in the range of  $10^{-8}$  F indicating the response of a passivating film at the Li/polymer electrolyte interface [3].

Nyquits plots for PEO films with the Triton X100 or the two siloxane surfactants show that these molecular layers appear to prevent the formation of an ever-increasing second semicircle associated with the passivation layer due to a non-stable interface.

Table 1 also presents data as to whether or not the listed molecular films will prevent passivation, thus stabilizing the lithium/polymer electrolyte interface. This will

be helpful in discussion of the present work. All molecules having a  $-(\text{CH}_2\text{CH}_2\text{O})-$  tail are able to stabilize the interface. Only the adsorbed alcohol and the carboxylic acid are not able to perform this function. Since past work was on ordered hydrocarbon chains that stabilized the interface [2], an ATR FT-IR investigation of  $\text{CH}_2$  chain order was done for the alcohol and the carboxylic acid. Figure 4.1 shows IR data for the  $\text{CH}_2$  stretching region for the alcohol and acid adsorbed on the surface (top spectrum in both a and b) and for the pure compounds, which are solid, semi-crystalline, waxy materials (bottom spectra a and b). The antisymmetric and symmetric  $\text{CH}_2$  stretching modes in the pure compounds are seen at frequencies of 2915 and 2847  $\text{cm}^{-1}$  respectively. These are indicative of well ordered, crystalline hydrocarbon tails [4] and would be expected to be seen in these semi-crystalline solids. In our previous work [2] vibrational modes of approximately the same frequency have been seen for molecules adsorbed on the polymer surface. This is indicative of bordered, self-assembled hydrocarbon tail that certainly could be one condition necessary for interface stabilization. However, the top spectra in a and b for the adsorbed alcohol and acid show that the antisymmetric and symmetric stretching modes have increased in frequency from 5-8  $\text{cm}^{-1}$ . An increase in frequency to this degree has been attributed to disorder in the hydrocarbon chains due to more gauche conformations in the hydrocarbon tail [5].

Knowing that the alcohol and acid are adsorbed on the surface and that the hydrocarbon tails of such molecules would tend to self-assemble, a reason for their apparent disorder is necessary to understand these systems. A possible explanation for this lack of order could be in the adsorption density. Data from previous work [1,2] and this work show that molecules with  $-(\text{CH}_2\text{CH}_2\text{O})-$  tails readily adsorbed on the surface and form what seem to be continuous self-assembled hydrocarbon surfaces. These tails must adsorb to the surface by intermingling tightly or adsorbing closely with electrolyte surface PEO polymer electrolyte molecules, resulting in the hydrocarbon portion of the molecule's ability to self-assemble in an ordered layer. Here it seems that the alcohol and the acid are able to adsorb on the surface, but perhaps to only certain polar regions where an ether oxygen in the polymer backbone is exposed on the polymer electrolyte surface. These adsorption sites may be too far apart for the hydrocarbon tails to self-assemble properly resulting in the disordered chains shown by the IR spectra. Indeed, areas may exist where the adsorbed molecules are so far apart that the lithium can easily "see" the polymer electrolyte surface resulting in the reactions occurring that are responsible for interface destabilization. Interestingly, it is hard to imagine that the Triton X100 and the siloxane surfactants would form an ordered structure on the surface because of the branching and bulky pendant groups on these molecules. One would expect what is commonly called a "brush" surface that has little order would be the surface structure of preference. However, having the  $-(\text{CH}_2\text{CH}_2\text{O})-$  tails adsorb densely on the polymer electrolyte surface results in the brushes being very closely packed, albeit disordered, presenting a continuous protective surface that the lithium experiences. These interfaces are thus also stabilized.

#### 4.4. CONCLUSIONS

Molecules having the general form  $R-(CH_2CH_2O)_m-H$  can adsorb on PEO polymer electrolyte surfaces. Adsorption of these molecules stabilize the lithium/polymer electrolyte interface whether the R group is a long, straight hydrocarbon tail capable of forming an ordered self-assembled structure or a branched hydrocarbon or a siloxane with bulky hydrocarbon groups that form a brush structure. The critical factor appears to be that the R group forms a continuous layer that does not allow the lithium to "see" the polymer electrolyte surface, preventing reactions from occurring that can destabilize the interface. While an R-OH and an R-COOH, where R was a long, straight chain hydrocarbon, were found to adsorb on the surface, they did not stabilize the interface. This was attributed to a low adsorption density resulting in the inability of the R groups to form a continuous protective molecular layer. These adsorbed molecular protective layers placed on "dry" polymer electrolytes, as studied here, or on gel polymer electrolyte systems have the potential to stabilize both the anode and cathode interfaces. Future work will investigate the use of this technique for interface stabilization using various anode materials such as graphite and different cathode systems.

#### 4.5. References

1. R. N. Mason, M. Smith, T. Andrews, and D. Teeters, *Solid State Ionics* **118**,129 (1999).
2. M. Le Granvalet-Mancini, L. Honeycutt, D. Teeters, *Electrochim. Acta*, **45**, 1491 (2000).
3. P. G. Bruce in *Polymer Electrolyte Reviews* Volume 1, (Edited by J. R. MacCallum and C. A. Vincent) p. 237, Elsevier, London (1987).
4. F. Bensebas, T. H. Ellis, E. Kruus, R. Voicu, and Y. Zhou, *Langmuir*, **14**, 6579 (1998).
5. R. G. Snyder, H. L. Strauss, and C. A. Elliger, *J. Phys. Chem.* **86**, 5145 (1982).

#### 4.6. Figures

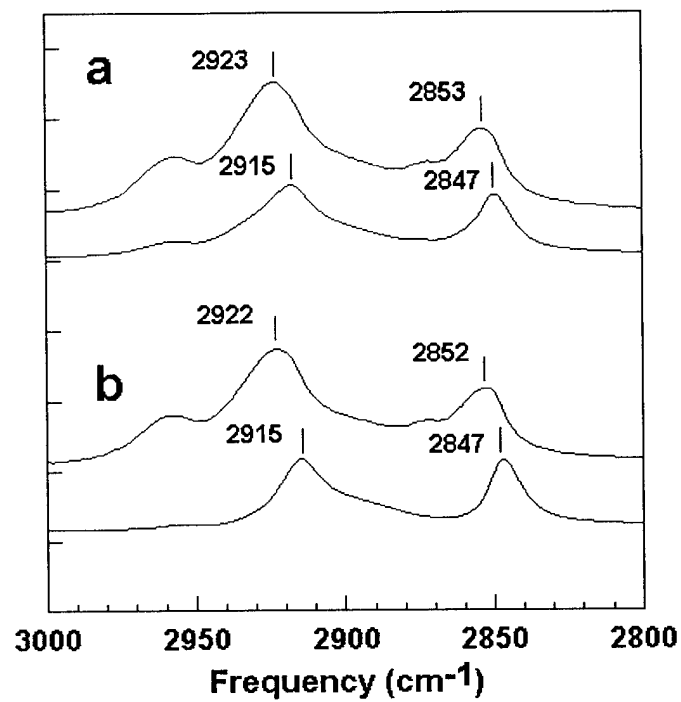


Figure 4.1

## **Chapter 5. Modeling of Passivation of Lithium Electrode in the Presence and Absence of Self-Assembled Molecular Layers at the Electrode/Polymer Electrolyte Interface**

### **5.1. Introduction**

In this part of our work the theory of a microelectrode array [1,2] has been applied to the passivated lithium surface. This approach can give useful insights into the structure and growth mechanism of the passivation layer. It also helps to evaluate the viability of using SAMs as protection against passivation of lithium surfaces in lithium batteries.

### **5.2. Experimental**

The symmetric lithium cells Li/Polymer Electrolyte/Li were made from two lithium electrodes. The electrodes (area =  $1.609\text{cm}^2$ ) were punched out from 0.0125 inch thick lithium ribbon obtained from Aldrich chemicals. The lithium was always stored in the glove box in argon atmosphere. The polymer electrolyte was cut as square pieces ( $1.5 \times 1.5\text{cm}^2$ ) from films made in our laboratory. The electrolyte films were made from PEO (MW = 900,000) and lithium trifluoromethanesulfonate (triflate) salt, and the concentration of lithium in the polymer was 15:1 ether oxygens to one lithium ion. The complete procedure for making and storing the films and the cells can be found in Chapter 1 [3,4]. The thickness of the films ranged from 100 to 130  $\mu\text{m}$ . PEO electrolytes with self-assembled molecular layers adsorbed on the surface were prepared as described previously in Chapter 1 and in the literature [3,4]. Semicrystalline wax from Petrolite Specialty Polymers, described as  $\text{H}-(\text{CH}_2)_{32}-(\text{CH}_2-\text{CH}_2-\text{O})_{10}-\text{H}$ , was used to form the self-assembled molecular layers. Squares ( $2 \times 2\text{cm}^2$ ) cut from nickel foil (0.125mm thick) from Aldrich chemicals were used as current collectors. The cells were assembled as Ni/Li/Polymer Electrolyte/Li/Ni in a glove box under argon purge and placed in a sample holder. The sample holder was then placed in a glass tube fitted with rubber cork. The glass tubing was evacuated and placed in an oil bath at a temperature of  $75^\circ\text{C}$  controlled to  $\pm 0.01^\circ\text{C}$ . The cells were cycled using a MACCOR battery cycler. Each cycle consisted of a charge step at  $150\text{ }\mu\text{A cm}^{-2}$  for 30 minutes followed by a discharge at the same current density for another 30 minutes. After 10 such cycles, impedance measurements were made using a Hewlett-Packard 4914-A a.c. impedance/gain phase analyzer. The impedance data were obtained in a 100Hz-40MHz frequency range.

### **5.3. Results and Discussion**

#### **5.3.1. Microelectrode Array Model of Passivation Layer**

A passivated lithium electrode can be thought of as a surface consisting of active and passive sites distributed over the whole area similar to a microelectrode array. As such the theory of an ideal microelectrode array can be used to calculate electrode coverage by the passivation layer. To apply this model we assumed that the



electrode/electrolyte interface is free from passivation as soon as the cell is assembled. AC impedance measurements are made at successive times as described in the experimental section.

Equations for the impedance response of microelectrode array have been derived and can be found in the literature [1,2]. The faradaic impedance of a microelectrode array consists of the in-phase resistive component  $Z'_f$  and the out of phase capacitive component  $Z''_f$ . The diffusion of the electroactive species to an active site of the microelectrode array is non-linear. This non-linear diffusion problem is mathematically equivalent to a linear diffusion problem coupled with a first-order homogeneous chemical reaction. Equations for the latter problem and their derivations can be found in the literature [5-8].

If we assume that the concentrations of the oxidized and reduced forms of the redox couple are equal and that their diffusion coefficients are equal, the two components of the faradaic impedance are given by

$$Z'_f = R_{ct}/(1 - \theta) + \sigma/\sqrt{\omega} + (\sigma/(1 - \theta))\{[(\omega^2 + q^2)^{1/2} + q]/[\omega^2 + q^2]\}^{1/2} \quad (5.1)$$

$$Z''_f = \sigma/\sqrt{\omega} + (\sigma/(1 - \theta))\{[(\omega^2 + q^2)^{1/2} - q]/[\omega^2 + q^2]\}^{1/2} \quad (5.2)$$

where  $R_{ct}$  is the resistance to charge transfer,  $\theta$  is the electrode coverage,  $\sigma$  is the Warburg impedance slope,  $\omega = 2\pi f$  is the angular frequency, and the term  $q$  is defined as below.  $R_{ct}$ ,  $\sigma$ , and  $q$  can be defined as

$$R_{ct} = (RT/F)/(FAk^0C) \quad (5.3)$$

$$\sigma = [\sqrt{2(RT/F)}]/[FAC\sqrt{D}] \quad (5.4)$$

$$q = [2D]/[R_o^2\theta(1 - \theta) \ln(1 + 0.27/(1 - \theta)^{1/2})] \quad (5.5)$$

here  $C$  is the concentration of either the oxidized or reduced form of the redox couple,  $A$  is the total geometric area of the electrode surface,  $D$  is the diffusion coefficient,  $k^0$  is the rate constant of the charge transfer reaction,  $R_o$  is the radius of the inactive sites, and  $R$ ,  $T$  and  $F$  have their usual significance.

A plot of  $Z'_f$  vs.  $\omega^{-1/2}$  shows two linear regions, one in the high frequency region and the other in the low frequency region, intersecting at the transition frequency. The equations describing the two linear regions respectively can be derived by setting  $\omega \gg q$  and  $\omega \ll q$  in equation (1). This procedure yields the following expressions:

$$Z'_f = R_{ct}/(1 - \theta) + \sigma / \sqrt{\omega} + \sigma / [(1 - \theta) \sqrt{\omega}] \text{ (high frequency region)} \quad (5.6)$$

$$Z'_f = R_{ct}/(1 - \theta) + \sigma / \sqrt{\omega} + [\sigma R_a(0.72/D)^{1/2} / (1 - \theta)] \text{ (low frequency region)} \quad (5.7)$$

where  $R_a$  is the radius of the active sites. The transition frequency where the two lines intersect is given  $\omega = q/2$ . As can be seen from equation (7) the slope of the high frequency line for a clean electrode ( $\theta = 0$ ) can be used to calculate  $\sigma$ . This value of  $\sigma$  can be used to calculate  $\theta$  for the passivated surface. Further more, the radius of the inactive sites,  $R_o$  can be calculated by using equation (5) and noting that at the transition frequency  $\omega = q/2$ . The sizes of active sites,  $R_a$  can then be calculated using the following relation:

$$(1 - \theta) = R_a^2 / R_o^2 \quad (5.8)$$

Figure 5.1 shows the time variation of  $(1 - \theta)$  obtained by the above analysis. The active surface area  $(1 - \theta)$  is seen to decrease rapidly to about 60% in the first 48 hours for the case of the interface not protected by SAMs. Then it plateaus at close to 45%. This is consistent with the passivation layer growing rapidly initially and then forming a compact layer that remains relatively constant with time. Such a behavior, an increase in interfacial resistance with time, has been reported [9]. However, to our knowledge, there have been no reports of quantifying the extent of passivation in terms of the surface area rendered inactive. For the case of the interface protected by SAMs it can be seen that the active surface area decreases to about 70% in 24 hours but recovers back to about 80% and no further deterioration of the surface is evident. The recovery is probably due to the rearrangement of surface molecules. It is evident from the plot that the interface does not change much with time and remains stable due to the protection offered by SAMs present at the interface. Calculation of the sizes of active and inactive sites as outlined earlier reveals that the sites are of the order of a few tens of nanometers.

### 5.3.2. AFM Images

The left image in Figure 5.2 shows the AFM image ( $1.5 \mu\text{m} \times 1.5 \mu\text{m}$ ) of a lithium surface that was exposed to a PEO electrolyte for 3 days. Passivated sites can be seen as crystal-like dendritic structures. The sizes of the sites seen in the image are of the same order of magnitude as those calculated from the microelectrode array theory. Figure 5.2 shows the image of a lithium surface ( $1.5 \mu\text{m} \times 1.5 \mu\text{m}$ ) exposed to a PEO electrolyte covered by a layer of SAMs. The features corresponding to passivated sites are of smaller size and much more sparsely distributed over the surface. The sparse distribution of smaller passivated sites agrees well with the higher active surface area predicted by the microelectrode array model seen in Figure 5.2 for the case of the SAM protected interface.

It is clear from the above results that SAMs stabilize the interface by inhibiting the growth of passivation layer. However, the underlying reason for the observed behavior is not clear. It is known that the passivation layer builds up as a result of two reactions. One is the reaction of lithium with the PEO surface and the other is a reaction between lithium and the anion of the electrolyte doping salt [10]. It is obvious that the contact between lithium and the PEO surface is greatly reduced by the presence of a SAM

layer at the interface. This helps in reducing the extent of passivation. It is conceivable that the PE tails might hinder the movement of the anion. This might also contribute to the increased stability of the interface protected by SAM. Further experiments are being conducted in our laboratory to elucidate this mechanism.

#### 5.4. Conclusions

It has been shown that SAMs protect the lithium/electrolyte interface during cycling. The extent of protection achieved has been quantified using the microelectrode array theory. The calculated sizes of active and inactive sites compare well on the order of magnitude scale with those seen in the AFM images.

#### 5.5. References

1. H. O. Finklea, D. A. Snider and J. Fedyk, *Langmuir*, **9**, 3660 (1993).
2. K. Tokuda, T. Gueshi, and H. Matsuda, *Electroanal. Chem.*, **102**, 41 (1979).
3. R. N. Mason, M. Smith, T. Andrews, and D. Teeters, *Solid State Ionics* **118**, 129 (1999).
4. M. Le Granvalet-Mancini, L. Honeycutt, D. Teeters, *Electrochim. Acta*, **45**, 1491 (2000).
5. H. Gerischer, *Z. Phys. Chem.*, **198**, 286 (1951).
6. A. J. Bard and L. R. Faulkner, in *Electrochemical Methods: Fundamentals and Applications*, John Wiley & Sons, New York (1988).
7. D. E. Smith, in *Electroanalytical Chemistry*, A. J. Bard, Editor, p. 1-155, Marcel Dekker, New York (1966).
8. M. Sluyters-Rehbach and J. H. Sluyters, in *Electroanalytical Chemistry*, A. J. Bard, Editor, p. 1-128, Marcel Dekker, New York (1970).
9. P. G. Bruce in *Polymer Electrolyte Reviews Volume 1*, (Edited by J. R. MacCallum and C. A. Vincent) p. 237, Elsevier, London (1987).
10. C. A. Vincent, *Prog. Solid State Chem.*, **17**, 145 (1987).

## 5.6 Figures

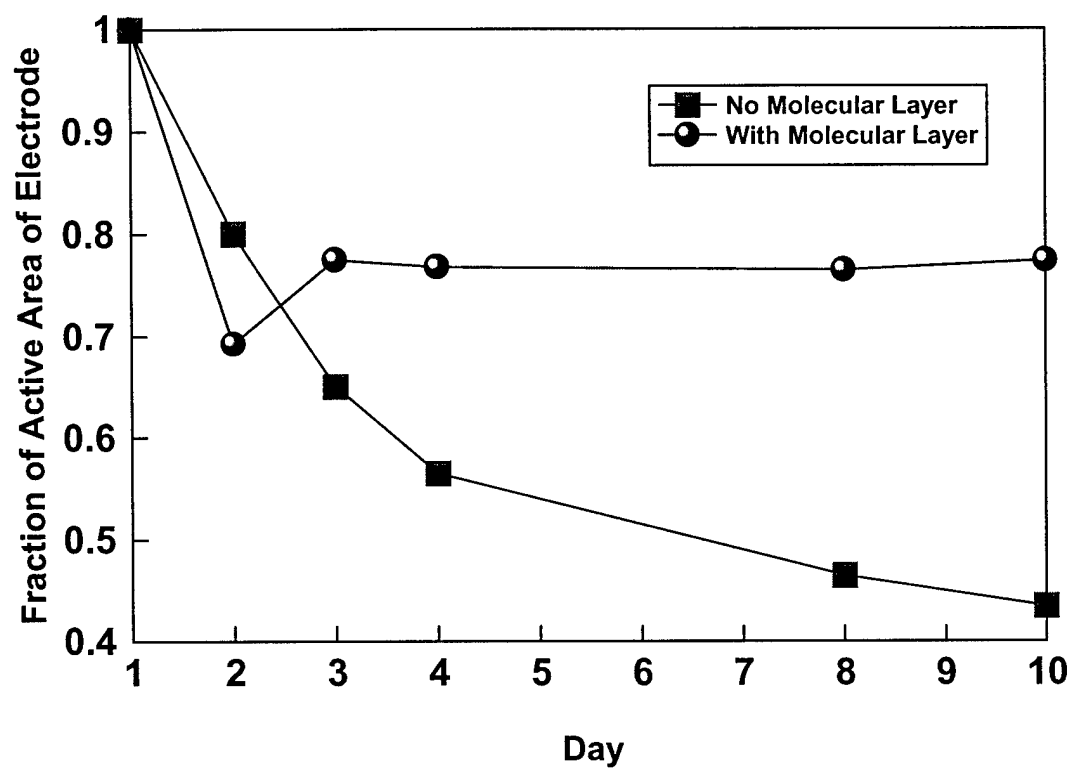


Figure 5.1

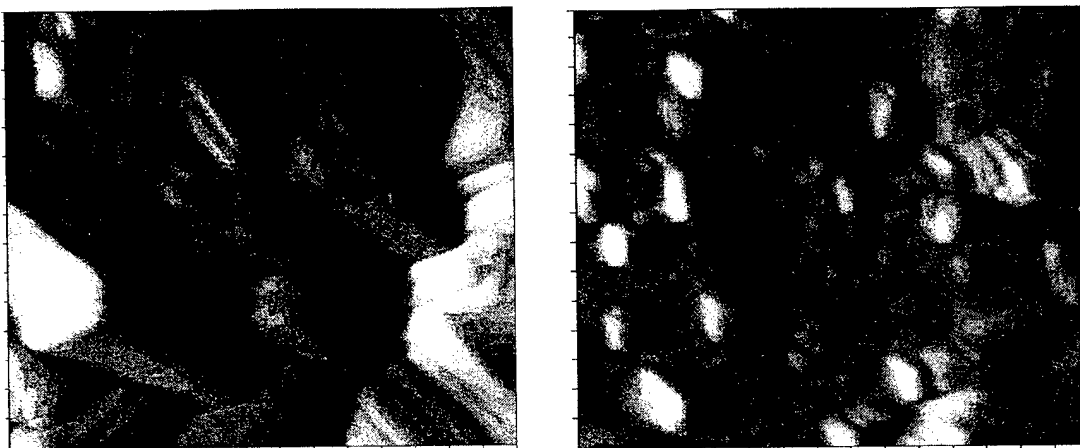


Figure 5.2

## **Chapter 6. Scanning Probe AC Impedance Spectroscopy: A New Method to Study Electrode and Electrolyte Interfaces.**

### **6.1. Introduction**

Understanding properties at the micro or nanoscale can often be of great importance in comprehending similar properties at the macroscale. However, microscale and often to a greater extent nanoscale properties can differ quite dramatically from their macroscale counterparts. Past work in our laboratory has focused on the macroscale characterization of the polymer electrolyte / lithium electrode interface, which is of significant importance to the performance of lithium-ion batteries [1,2]. Currently, however, there exists no good way to analyze surface or bulk electrical characteristics of these polymer electrolytes at the nanoscale. This necessitates the need to develop a nanoscale technique that can be used in the characterization of these films.

As electrochemical systems, such as batteries, become ever smaller, developing techniques that allow sample characterization at the size of the systems of interest is of the utmost importance. In the last decade or so, the ability to study electrochemical surfaces and interfaces with high lateral resolution has been greatly enhanced by the use of scanning probe microscopy. Techniques such as conducting-atomic force microscopy [3], and current-sensing atomic force microscopy [1], take advantage of the high-resolution imaging capabilities of the AFM and the ability of the AFM probe to be used as an electrode. In this paper we use polymer electrolyte films to show that the combination of scanning probe microscopy and alternating current (a.c.) impedance spectroscopy offers an interesting new way to characterize conducting systems at the nanoscale.

A.C. impedance spectroscopy is a traditional technique used in studying the properties of electrochemical systems [4]. This technique is particularly suited to studying polymer electrolyte films. Sandwiched between inert electrodes, polymer films act like simple electrochemical cells, and bulk electrical properties are readily determined.

Atomic force microscopy (AFM) is used to collect the nanoscale a.c. impedance data. Previous research has been done where measurements with probes as small as 5 – 10  $\mu\text{m}$  in diameter were used [5-7]. Today, AFM probes routinely have tip diameters of 20 nm or smaller and are readily available. These sharp probes provide a dramatic improvement in surface resolution and allow for true nanoscale impedance measurements. With a metal or metal-coated AFM probe, the probe-tip acts as a nanoelectrode, which can be used to examine the conductivity of nanoscale regions or features on the surface. The AFM also allows for control over tip/surface contact parameters, such as tip force, which is necessary to collect electrochemical information on the solid polymer films.

## 6.2. Experimental

### 6.2.1. Film preparation

All films were made using 900 000 molecular weight poly(ethylene) oxide from Aldrich Chemical and lithium triflate (Aldrich) with a 15:1 ratio of ether oxygen to lithium. The polymer and salt were dissolved in acetonitrile (Fisher) providing the working solution for film preparation. A complete procedure for film production has been previously described in the literature [8].

Two different types of PEO-lithium triflate films (here-to-for referred to as PEO films) were examined in this study. The first was a drop cast film where a small amount the PEO solution was dropped by pipette on a piece of Ni-foil. The solution was allowed to air dry forming a film on the Ni-foil with a thickness ranging from 6 $\mu\text{m}$  – 15 $\mu\text{m}$ . The film was further dried in a vacuum oven at a temperature of 50 °C.

The second film type consisted of a PEO filled porous polycarbonate (PC) membrane (Osmotics, Inc.). The pore diameter for the PC membrane was 0.1 $\mu\text{m}$  and the membrane thickness was approximately 6  $\mu\text{m}$ . A thin layer of PEO solution was poured into a Teflon lined container after which the PC membrane was carefully floated on top of the solution. The container was placed in an airtight desiccator and a slight vacuum was applied. In the presence of a vacuum the solution was pulled up through the membrane filling the pores and coating the top of the membrane with a thin film of PEO. After approximately 10 minutes the vacuum was released and the sample was allowed to completely dry under continuous nitrogen flow. The resultant film consisted of a PC membrane incorporated within the thin polymer film, with PEO filled pores and a thin polymer layer on the top of the membrane. The bottom side of the membrane was typically coated with a thicker PEO film as a result of floating on the polymer solution during film formation. The polymer filled polycarbonate membrane film (PEO-PC) was adhered to Ni-foil by wetting the foil with a small drop of the PEO solution, followed by placing the PEO-PC film bottom side down on the foil. The PEO-PC films were also further dried under vacuum at 50 °C. A more complete procedure regarding the PEO-PC films is described elsewhere [9].

Nickel foil ( 0.5 mm thick) was used as the substrate/electrode when mounting the PEO films, as it was readily available in our laboratory. Issues concerning the use of Ni as an electrode material, rather than more inert gold or platinum, will be discussed later.

### 6.2.2. Instrumentation

Surface imaging was conducted using a Molecular Imaging PicoSPM atomic force microscope (AFM) in contact mode. Silicon AFM probes (Nanosensors) with nominal force constant of approximately 0.2 N/m and typical tip diameters of 20 nm were used for all reported data. The tips were sputter coated (Cressington 208HR sputter coater) with 3-4 nm of chromium followed by 35-40 nm of gold for electrical contact. The chromium allows for better gold adherence to the probe tip. This proves critical as the tip was used for both imaging and impedance measurements, the latter of which requires intimate surface contact. On the soft polymer films tip durability was not a problem and the tip

could be used for extended periods of time with little change in performance. Measurements on harder materials, such as the Ni foil, abraded the metal coating much more rapidly, sharply reducing the usable lifetime of the tip for impedance measurements.

Impedance spectroscopy measurements were conducted using an HP 4194-A ac impedance-gain phase analyzer and a Solatron 1255 gain/phase analyzer with the 1287 electrochemical interface. Typical data was collected over a range of 400MHz – 100 Hz and 400MHz – 0.01 Hz for the HP and Solatron instruments respectively.

Macroscale impedance measurements were conducted for direct comparison with those by AFM. Macroscale measurements were performed using a test cell in which the polymer films were sandwiched between two circular stainless steel electrodes with an area of 0.5 cm<sup>2</sup>. Impedance measurements at the nanoscale were conducted with the tip of the AFM probe. This was accomplished after surface imaging by positioning the tip over the feature or area of interest and applying force to the tip to ensure good surface contact. Once tip/surface contact was made, impedance measurements could begin. For both macro and nanoscale measurements electrical connections to the impedance analyzer was accomplished with simple wire attachments to the various electrodes. All experiments were conducted under ambient conditions at room temperature.

### 6.3. Results and Discussion

#### 6.3.1. Nanoscale a.c. impedance measurements

The images and curves in Figure 6.1 demonstrate the success in coupling the atomic force microscopy and a.c. impedance techniques. Figures 6.1a and 6.1c are AFM images of the cast PEO and PEO-PC films respectively. The upper right corner of Figure 6.1b shows the morphology of the polycarbonate membrane prior to being filled and coated with PEO. The four tiles of Figure 6.1a show the structure of the PEO film sampled at four *different locations* over the same film. Between each run, the film was moved under the AFM tip to ensure sampling in different regions. Impedance data for Figure 6.1a are shown in Figure 6.1b. It is observed that the ion conductivity varies greatly from region to region. Image (i) of Figure 6.1a shows almost no conductivity as demonstrated by the large resistance of the corresponding impedance curve. Conversely, image (iii) shows the opposite behavior and exhibits fairly high conductivity as compared to the area in image (i).

The impedance data in Figure 6.1d show the resistance values at four different points *within the scan area* of the image in Figure 6.1c. To obtain this data the sample was held stationary and the AFM probe was moved from point to point within the image. The overlapping impedance curves (ii) of Figure 6.1d show that ion conductivity varies little over the entire area of the image. Curve (i) of Figure 6.1d is the impedance curve for the uncoated polycarbonate membrane and exhibits no conductivity as compared to the PEO coated membrane.

In general, impedance data similar to curve (i) of Figure 6.1b, is representative of data collected for the majority of the areas sampled for these films - most of the regions exhibit very low conductivity. PEO films are known to be heterogeneous with respect to their ion conducting capabilities. Amorphous regions are known to be more conductive



than crystalline regions of the film [10-12]. The crystalline phase clearly dominates the structure of these films at room temperature as evidenced by the numerous areas that must be sampled before a conducting region is found. When considering the nature of the films and the size of the scans, it is not surprising that finding conducting regions is difficult. The largest scan area possible with our microscope is approximately 6800 nm x 6800 nm. The maximum possible area that can then be examined is 46  $\mu\text{m}^2$ . While large as compared to typical nanoscale measurements, this minute area becomes ever smaller when trying to locate conducting regions of the sample. Figure 6.1b further shows the heterogeneous nature of these films, exhibiting a wide range of conductivities over different regions. This variation may be attributed to the degree of crystallinity in that particular region. It may also be due to inhomogeneous distribution of the conducting salt during film formation. Regions with differing salt concentrations will most assuredly exhibit different ion conductivities.

Much less frequently found were regions of the films with relatively high conductivities. Conduction in such regions appears to be fairly constant over the entire scan area. This was true for all regions with relatively high conductivities. This indicates that conductive regions of these films are at least 46  $\mu\text{m}^2$  in size. Due to the configuration of our microscope we were not able to determine the lateral extent of these conducting regions.

The ability to differentiate regions of high and low conductivity at the nanoscale demonstrates the unique capabilities of the AFM for measuring impedance data. While not shown here, we have also successfully obtained data where both conducting and nonconducting phases were present within the same scan area. Because of the overwhelmingly crystalline nature of the films, finding such areas is extremely difficult and many regions must be examined before an example is found. Impedance curves for such examples resemble those in Figure 6.1b the only difference being the data were obtained within the limits of a single scan area. The impedance curves for the coated and uncoated polycarbonate membranes in Figure 6.1d clearly demonstrate the ability of the AFM to differentiate regions of the surface using conductivity or impedance data.

### 6.3.2. Macro scale versus nanoscale measurements

To examine the capabilities of the AFM in performing impedance measurements, a comparison was made between the nanoscale and macroscale impedance data for the polymer films. The comparison between the AFM and the macroscale test cell is shown in Figure 6.2. Figures 6.2a and 6.2b are AFM images of a cast PEO and PEO-PC films respectively. The Nyquist plots for both macroscale measurements (Figure 6.2c) and nanoscale measurements (Figure 6.2d) show data for both the PEO film (curves labeled as (i)) and the PEO-PC film (curves labeled as (ii)).

Both macroscale and nanoscale plots exhibit the same basic shape with no differences except for the magnitudes of the impedances. In both cases the PEO-PC films showed slightly higher impedance values, probably due to the confinement of the polymer electrolyte in the pores of the polycarbonate membrane [9,13]. The lack of any difference in the shape of the curves indicates the vast difference in electrode size ( $\text{cm}^2$  for the macroelectrode to  $\text{nm}^2$  for the AFM probe) does not affect the impedance measurement.

Impedance values collected with the AFM, however, are typically much higher than those of the test cell. This is most likely due to the difference in electrode area.

Surprisingly, the impedance values for both films in Figure 6.2 only increased approximately two orders of magnitude when going from the macro to nanoscale electrode. The corresponding decrease in electrode area, though, is in the range of ten orders of magnitude. Classically the resistance scales inversely with the electrode area, so the apparent conductivity of the samples in the nanoscale measurements is larger than would be expected. The heterogeneous nature of ion-conduction in the PEO films may offer an explanation for the large nanoscale impedance. Macroscale electrodes measure the ion-conductivity over a large surface area simultaneously sampling both crystalline and amorphous regions of the films. The resultant impedance can be thought of as an average impedance of the various phases comprising the film. The resultant impedance is small because many conducting amorphous regions are being sampled at the same time. The small size of the nanoelectrode almost ensures that only one phase will be sampled for each measurement. When an amorphous region of the PEO film is found the conductivity appears larger than expected because the tip is sampling only a conductive region.

Close examination of the Nyquist plots in Figure 6.2 allows for more direct comparison between macro and nanoscale measurements. Using the data in Figure 6.2c, the bulk resistance for the PEO sample was determined to be approximately 1000  $\Omega$  for the macroscale test cell. This is much larger than would normally be expected for a PEO polymer electrolyte film. This was most probably due to the measurements being made under atmospheric conditions, the same conditions under which the AFM impedance data were collected, which allowed for direct comparison between the two experiments.

To gain a clearer understanding of the relationship between the resistance measured at the nanoscale through the AFM tip and bulk resistance of a polymer electrolyte film, we can use the well-known spreading resistance formula [14-18]

$$R_{\text{spread}} = 1 / 2d\sigma_{\text{bulk}} \quad (6.1)$$

Where  $R_{\text{spread}}$  is the resistance measured by a microelectrode or in this case the nanometer-sized AFM tip,  $d$  is the diameter of the tip and  $\sigma_{\text{bulk}}$  is the bulk specific conductivity of the electrolyte. Using a film thickness of 10  $\mu\text{m}$  and an area of 0.5  $\text{cm}^2$  for the macroelectrode, the bulk conductivity for the PEO film was calculated to be  $2 \times 10^{-4} \Omega^{-1} \text{m}^{-1}$ . Assuming the diameter of the tip is 20nm, the  $R_{\text{spread}}$  is calculated to be 125  $\text{G}\Omega$ .

From impedance data, like those for curves (i) of Figures 6.1c and 6.1d, the higher resistance values, which could be attributed to crystalline regions, were estimated to be in the range of  $10^4 \text{ G}\Omega$  and the low resistance values, which could be attributed to amorphous regions, were in the range of 1  $\text{M}\Omega$ . It is logical to expect that the  $R_{\text{spread}}$  calculated from equation 1 should lie between the two extreme values for the crystalline and amorphous phase, since the macroscale bulk measurements of this type measures conduction through both phases simultaneously. The value of 125  $\text{G}\Omega$  does lie within this range.

### 6.3.3. Instrumental effects on nanoscale impedance measurements

When performing impedance measurements with the nanoscale electrode, other instrumental properties must also be taken into account during the data collection process. One such property, inherent to the AFM, is the effect of probe force on the resultant impedance data. Figure 6.4 shows Nyquist plots for two separate experiments where the applied force on the AFM probe was increased between each run on a PEO-PC film. The tip was held stationary on the surface, and the probe was not retracted between runs to ensure that the same location was being examined. Increasing the voltage settings in the microscope software increased the tip force applied to the sample. At the voltage limit of our microscope, the tip force was increased slightly further by manually pushing the sample into the tip using the coarse screw adjustment on the microscope. A force curve was collected to translate voltage settings to approximate force values.

The Nyquist plots of Figure 6.3a show that at low applied tip force (curves (i) and (ii)) the impedance values do not change. As the tip force is increased the corresponding impedance values begin to decrease. When the voltage limit of the instrument is reached and the tip is manually forced into the surface, the impedance curves reach their lowest values. It was found that manually increasing the tip force further had no effect on subsequent impedance values.

Contrary results were found when the experiment was repeated on a different area of the same sample. The results of this experiment (Figure 6.3b) showed that an increase in applied tip force had no effect on the observed impedance values. Similar experiments conducted on both PEO and PEO-PC films provided the same results. In some areas, changing the applied tip force affected the impedance data; in others it had no effect. Further, from region to region the degree to which the applied force affected the impedance values also varied.

Interestingly, the cause of the above observations may be due to film characteristics other than conductivity. From the AFM images it is observed that the films are far from flat and exhibit quite rough surface structure. Data like those in Figure 6.3a might be explained by assuming the tip is probing an area that is not flat directly beneath it. In the absence of a flat surface, it cannot be assumed that the entire surface area of the electrode is in contact with the sample. This would cause an increase in the measured impedance. As the probe force is increased, the tip will make more intimate contact with the surface resulting in increased contact area and decreased impedance. Data as in Figure 6.3b may result when the surface is relatively flat beneath the tip and good surface contact is made even at low applied forces. Such an example may not show any change in impedance values due to no significant increase in tip/surface contact area as force is varied. This explanation would also hold for examples in-between the above cases, with impedance depending on the surface structure.

Decreased impedance values would also occur if the tip were able to deform the surface being probed. On "soft" areas of the film, the tip may penetrate or indent the surface as probe force is applied. Doing so would increase the contact area as the edges or sides of the tip would now also be in contact with the film. In conducting regions of the film the increase in surface area could significantly affect impedance values.

The key point to the above explanations is that applied tip force does not directly cause a change in impedance; rather changing the force might result in a change in tip/surface contact area, with a subsequent change in impedance.

Other notable observations were also made in the course of these experiments. First, in regards to tip/surface contact area, it was found that impedance data was often very noisy in the limit of low frequency. This can be observed in the plots in Figure 6.3. In regions where measurements showed little or no conductivity, noise dominated the low frequencies. For highly conductive regions, it was found that increasing tip force resulted in reduced low frequency noise. Here too increased tip/surface contact area may factor in the decrease in noise at low frequencies. It must be pointed out that our electrical connections were made with non-shielded wires and the AFM was not protected from electro-magnetic interference. Using shielded cables and placing the AFM in a faraday cage may aid in limiting the noise in the low frequency range as well. It was also found that cleanliness of electrical contacts and the Ni-metal foil substrate was of critical importance. If the Ni-foil was not clean prior to sample mounting or the electrical contacts were dirty, impedance data was severely affected. The choice of Ni-foil as the polymer electrolyte substrate may have also imparted some error in the impedance measurements due to the native oxide that exists on the clean Ni surface. Due to the large impedances of the polymer films for these experiments, resistance due to the Ni-substrate was most likely negligible. Choosing more inert substrate materials such as gold or platinum will eliminate these concerns.

#### 6.4. Conclusions

We have successfully demonstrated that a.c. impedance spectroscopy can be conducted at the nanoscale by combining the technique with atomic force microscopy. Polymer electrolyte films were used as the material of interest in this work. It was shown that the AFM could differentiate regions of high and low ion-conductivity on the films. We compared the impedance data at the nanoscale with macroscale measurements and found no difference in the information obtained except for the magnitude of the impedance, with nanoscale measurements typically much larger than those at the macroscale. This was attributed to the large difference in area of the electrodes. After correcting for the size difference, nanoscale data were found to be consistent with macroscale data. Changing the force on the AFM probe was shown to have varying effects on impedance measurements. It was speculated that changes in the applied force cause changes in the tip/surface contact area, which in turn affects the impedance.

In this work our goal was to show that a.c. impedance data could be collected at the nanoscale. Where this combined technique will really show its usefulness, is not necessarily in measuring the impedance of nanoscale *regions of the surface*, but rather measuring the impedance for nanoscale *features on the surface*. Interesting and unique bulk properties, such as regions of increased/decreased conductivity, may manifest themselves through differences in surface structure. The work presented here shows the potential for this technique in the investigation of conductivity through specific surface sites and features.

## 6.5. REFERENCES

1. M. Le Granvalet-Mancini, T. Hanrath, D. Teeters, *Solid State Ionics*, 135 (2000) 283
2. M. Le Granvalet-Mancini, L. Honeycutt, D. Teeters, *Electrochimica Acta*, 45 (2000) 1491
3. J. V. Macpherson, J-P. Gueneau de Mussy, J-L Delplancke, *Electrochimical and Solid-State letters*, 4 (2001) E33
4. P. Bruce in: *Polymer Electrolyte Reviews*, Vol. 1, (Eds.) J.R. MacCallum and C.A. Vincent, Elsevier Applied Science, London and New York, 1987
5. J.W. Orton, P. Blood, in: *The Electrical Characterization of Semiconductors*, Academic Press, London, 1990, p. 53,
6. R. Holm, in: *Electric Contacts*, Springer-Verlag, Berlin, 1967, p. 16
7. J. Fleig, J. Maier, *Solid State Ionics*, 85 (1996) 9
8. R.N. Mason, M. Smith, T. Andrews, D. Teeters, *Solid State Ionics* 118 (1999) 129
9. S. Vorrey, D. Teeters, submitted for publication
10. F. M. Gray in: *Solid Polymer Electrolytes, Fundamentals and Technological Applications*, VCH, New York, 1991
11. F. M. Gray in: *Polymer Electrolytes*, RSC Materials Moographs, Cambridge, 1997, p. 8
12. P. Bruce in: *Solid State Electrochemistry*, Kluwer Academic Publishers, Boston, 1994
13. N. Korzhova, S.L. Fisher, M. Le Granvalet-Mancini, D. Teeters, *Proceedings of the American Chemical Society Division of Polymeric Materials: Science and Engineering*, 217<sup>th</sup> meeting of the ACS, (ACS, Washington D.C.) 1999, 618
14. F.L. Jones, in: *The Physics of Electrical Contacts*, Oxford University Press, Oxford, 1957, p. 15
15. J. W. Orton and P. Blood, in: *The Electrical Characterisation of Semiconductors*, Academic Press, London, 1990, p. 53,
16. R. Holm in: *Electric Contacts*, Springer-Verlag, Berlin, 1967, p. 16
17. J. Fleig, J. Maier, *Solid State Ionics*, 85 (1996) 9
18. S. Rodewald, J. Fleig, J. Maier, *Journal of the European Ceramic Society*, 19 (1999) 797

## 6.6 Figures

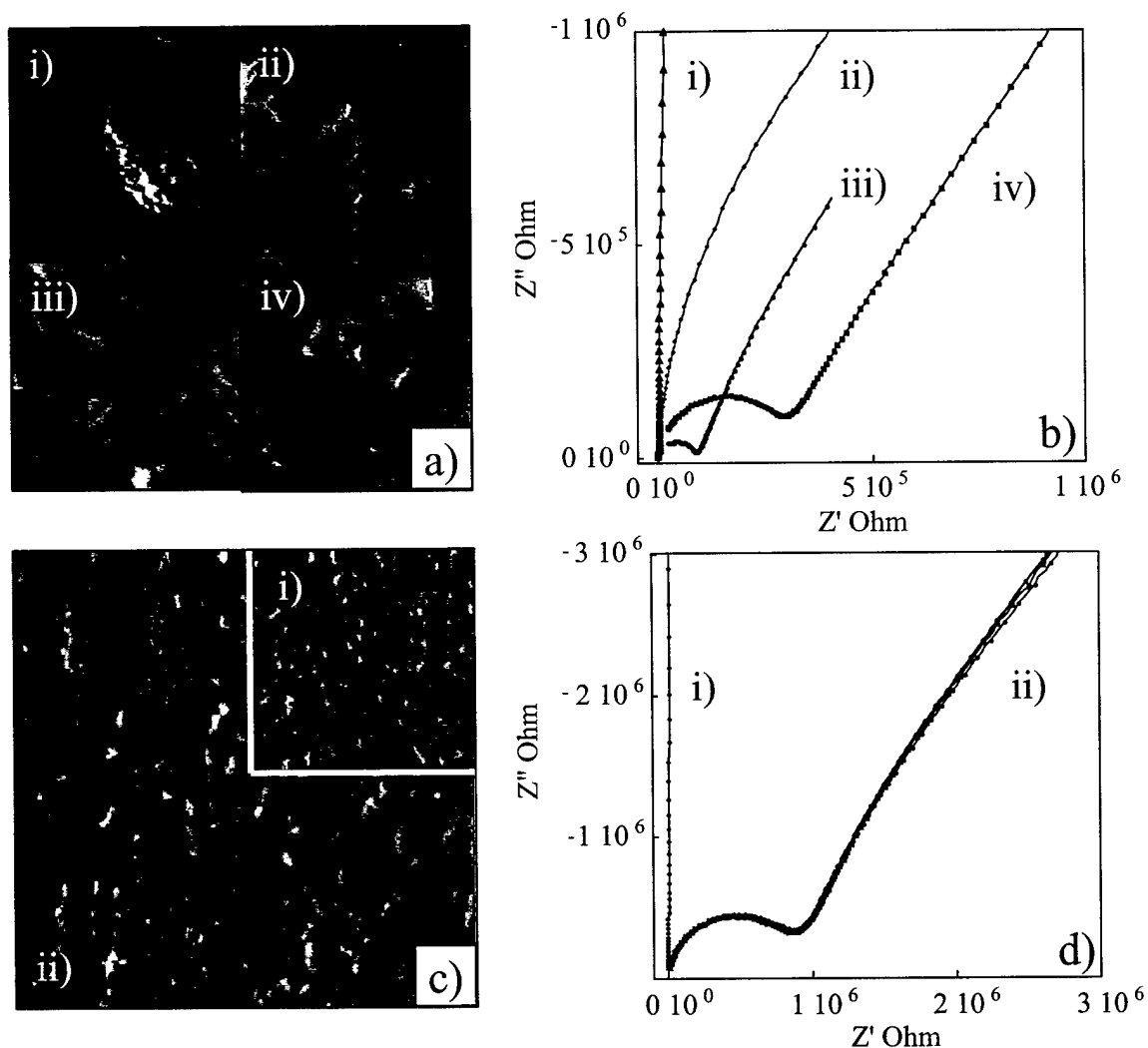


**Figure 6.1.** (a) AFM images of a PEO film at four different locations over the same sample. (b) Corresponding impedance data for the images shown in (a). (c) AFM image of a PEO coated polycarbonate membrane. The inset in the upper right corner is an image of the uncoated membrane. (d) Corresponding impedance data for the images shown in (c). The plots in (d) labeled as (ii) consist of data for four overlapping points probed within the area of image(c). The scan area for all images in (a) are  $3.8 \mu\text{m} \times 3.8 \mu\text{m}$ . Image (c) is  $6.8 \mu\text{m} \times 6.8 \mu\text{m}$ . The inset in (c) is to scale.

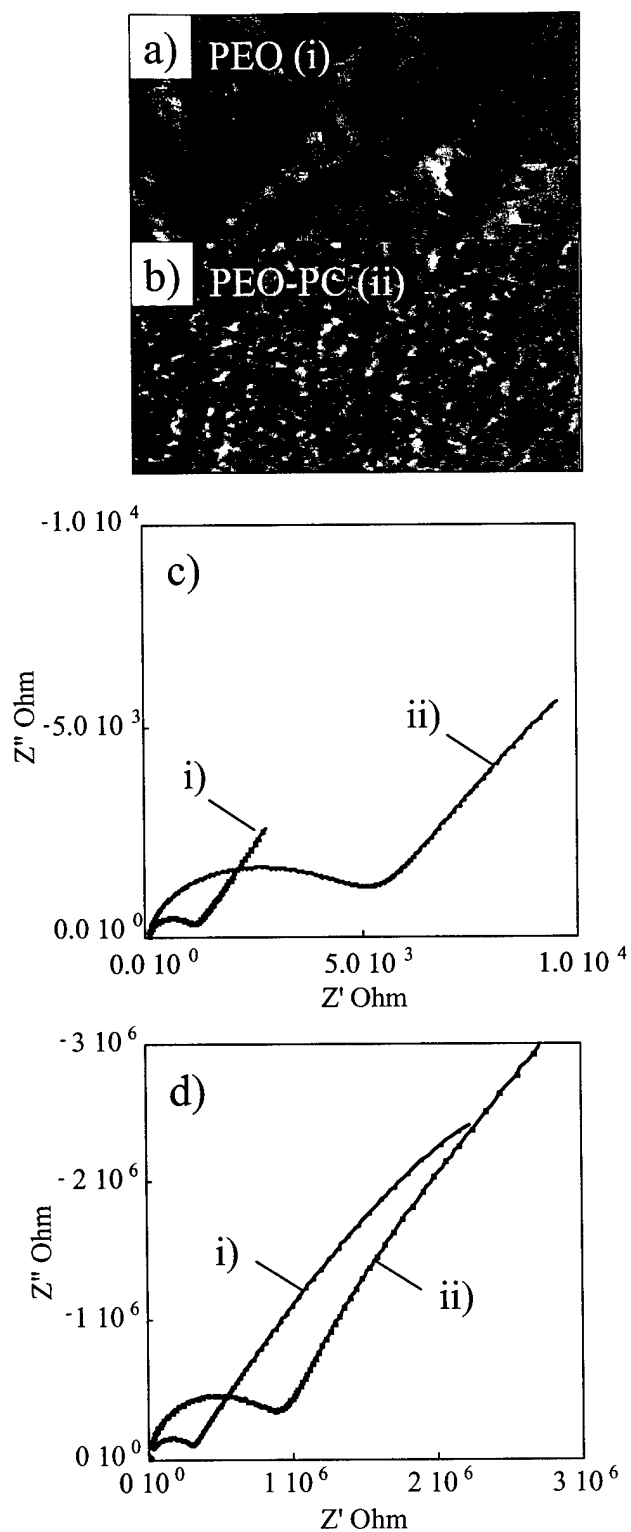


**Figure 6.2** (a) and (b) AFM images of a PEO and PEO-PC films respectively. (c) Macroscale a.c. impedance data. (d) Nanoscale a.c. impedance data. For both (c) and (d) the plots labeled as (i) are for the PEO film shown in (a). Plots labeled as (ii) are for the PEO-PC film shown in (b). The scan area for both images is  $6.8 \mu\text{m} \times 3.4 \mu\text{m}$ .

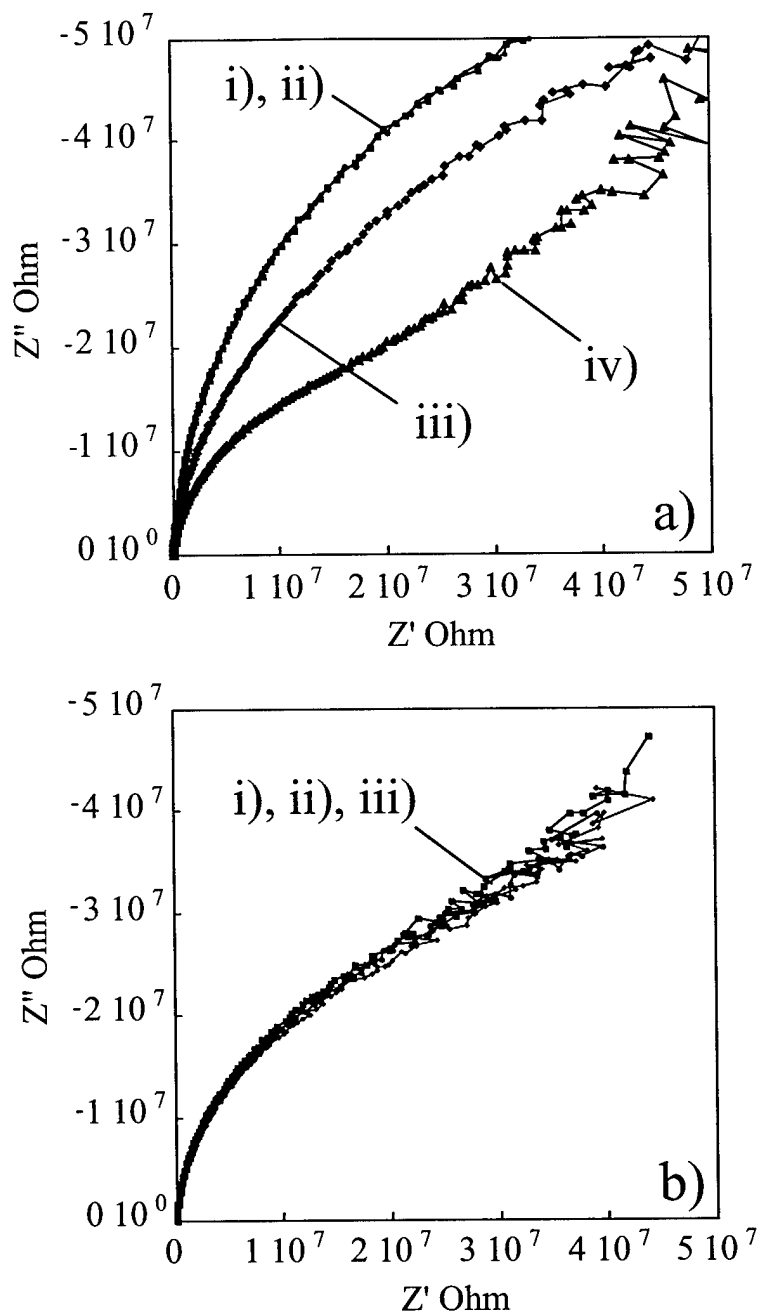


**Figure 6.3.** A.C. impedance data showing the effect of increasing probe force on impedance for a PEO-PC film. The force values in (a): i) 10nN, ii) 20nN, iii) 60nN, iv) <60nN. The data in (b) show three overlapping impedance plots. The force values in (b): i) 10nN, ii) 60nN, iii) <60nN. Plots (a)-iv) and (b)-iii) are impedance data for measurements where the tip force was manually increased past the limiting instrumental values. Force values for these points could not be precisely determined.



## VI. Personnel Supported

Maryline Le Granvalet-Mancini	Post Doctorial Fellow
William Redman	Research Associate
Robert Tipton	Research Associate
Shailesh Gadad	Ph.D. Graduate Student
Partha Puskur	Master's Student
Kalpna Bahunoothula	Master's Student
Shikpa Vangapally	Master's Student
Megan Papenfuss	Undergraduate
Nina Korzhova	Undergraduate
Lori Honeycutt	Undergraduate

## VII. Publications

M. Le Granvelet-Mancini, L. Honeycutt, and D. Teeters, "Characterization of Self-Assembled Molecular Layers at the Polymer Electrolyte/Lithium Electrode Interface," *Electrochimica Acta*, **45**, 1491 (2000).

M. Le Granvalet-Mancini, T. Hanrath, and D. Teeters, "Characterization of the Passivation Layer at the Polymer Electrolyte/Lithium Electrode Interface," *Solid State Ionics*, **135/1-4**, 283 (2000).

M. Le Granvalet-Mancini and D. Teeters, "The Effects of Chemical Composition of Adsorbed Molecular Layers on Lithium Electrode/Polymer Electrolyte Interface Stabilization," *Journal of Power Sources* **97-98**, 624 (2001).

S. Gadad and D. Teeters "Characterization and Stabilization of the Lithium/Polymer Electrolyte Interface: A Nanoscale Approach," in *Interfaces, Phenomena, and Nanostructures in Lithium Batteries Workshop*, Ed. A. Landgrebe, R. J. Klingler, (The Electrochemical Society, Pennington, NJ, December 2000) p. 288.

A. Layson, S. Gadad and D. Teeters, "Resistance Measurements at the Nanoscale: Scanning Probe AC Impedance Spectroscopy," Submitted, *Electrochimica Acta*.

## VIII. Participation/presentations at meetings, conferences, seminars, etc.

M. Le Granvalet-Mancini, T. Hanrath, and D. Teeters, "Characterization of the Passivation Layer at the Polymer Electrolyte/Lithium Electrode Interface," 12<sup>th</sup> International Conference on Solid State Ionics, Halkidiki, Greece, 1999.

N. Korzhova, S. L. Fisher, M. Le Granvalet-Mancini, and D. Teeters, "Ionic Conduction in Polymer Electrolyte/Microporous Membrane Composites," Symposium on Polymers for Batteries and Fuel Cells, The 217th National Meeting of the American Chemical Society, Anaheim, CA, March 21-25, 1999.

M. Le Granvalet-Mancini, L. Honeycutt, and D. Teeters, "Characterization of Self-Assembled Molecular Layers at the Polymer Electrolyte/Lithium Electrode Interface," Sixth International Symposium on Polymer Electrolytes, Hayama, Kanagawa, Japan, November 1-6, 1998.

L. Honeycutt, M. Le Granvalet-Mancini, and D. Teeters, "Infrared Spectroscopic Studies of Molecular Layers Adsorbed on Polymer Electrolyte Interfaces," The 217th National Meeting of the American Chemical Society, Anaheim, CA, March 21-25, 1999.

T. Hanrath, M. Le Granvalet-Mancini, and D. Teeters, "ATR-FTIR Investigation of Li-PEO Passivation Layers in Lithium Polymer Batteries," The 217th National Meeting of the American Chemical Society, Anaheim, CA, March 21-25, 1999.

D. Teeters, M. Le Granvalet-Mancini, L. Honeycutt, and T. Baird, "Passivation Protection at the Polymer Electrolyte/Lithium Electrode Interface," 43rd Oklahoma Pentasectional Meeting of the American Chemical Society, Ponca City, Oklahoma, 1998.

"Self-Assembled Molecular Layers at the Li/SPE Interface," Invited Talk, Bartlesville Section of the AIChE, Bartlesville, OK, Oct 31, 1999.

"Lithium Polymer Batteries," Invited Talk, Tulsa Section of IEEE, Tulsa, OK, November 9, 1999.

"Lithium Polymer Batteries," Invited Talk, Engineers Society of Tulsa, Tulsa, OK, Dec. 20, 1999.

"The Effects of Chemical Composition of Adsorbed Organic Molecular Layers on Lithium Electrode/Polymer Electrolyte Interface Stabilization," 10<sup>th</sup> International Meeting on Lithium Batteries, Como, Italy, May 28-June 2, 2000.

"Modeling of Passivation of Lithium Electrode in the Presence and Absence of Self-Assembled Molecular Layers at the Electrode/Polymer Electrolyte Interface," Symposium on Battery/Energy Technology Joint General Session as a part of the 197th Meeting of The Electrochemical Society, Toronto, May, 2000.

"Characterization and Prevention of Passivation at the Lithium/Polymer Electrolyte Interface," 45<sup>th</sup> Oklahoma Pentasectional Meeting of the American Chemical Society, Stillwater, Oklahoma, April, 2000.

"The Effects of Chemical Composition of Adsorbed Organic Molecular Layers on Lithium Electrode/Polymer Electrolyte Interface Stabilization," 10<sup>th</sup> International Meeting on Lithium Batteries, Como, Italy, May 28-June 2, 2000.

"Characterization of Organic Monolayers for Passivation Protection at the Lithium/Polymer Electrolyte Interface," The 219th National Meeting of the American Chemical Society, San Francisco, CA, March 25-29, 2000.

"Passivation Prevention Using Self-Assembled Molecular Layers at the Li/Solid Polymer Electrolyte Interface," Air Force Office of Scientific Research/Office of Naval Research Electrochemistry Science & Technology Review, Alexandria, VA, Feb. 14-16, 2000.

"Nanoelectrochemical Characterization of Polymer Materials Used in Batteries," The 221th National Meeting of the American Chemical Society, San Diego, CA, April 1-5, 2001.

"Resistance Measurements at the Nanoscale: Scanning Probe AC Impedance Spectroscopy," 8<sup>th</sup> International Symposium on Polymer Electrolytes, Santa Fe, New Mexico, May 19-24, 2002

#### **IX. Consultative and advisory functions to other laboratories and agencies**

Discussions with Hydro-Quebec concerning the results of this work. were conducted. Contacts have also been made with Maccor Company located in Tulsa, Oklahoma where an advisory/collaborative effort was established. Varitek of Carlesbad, California has contacted me concerning my work with molecular level films to stabilize the lithium/polymer electrolyte interface. I have had several discussions with their researchers.

#### **X. Inventions, or patent disclosures**

There have no inventions or patent disclosures.

#### **XI. Honors/Awards**

Dale Teeters, the PI, was named a Camille and Henry Dreyfus Fellow based on his research with students.

M. Le Granvalet-Mancini, T. Hanrath, and D. Teeters, "Characterization of the Passivation Layer at the Polymer Electrolyte/Lithium Electrode Interface," 12<sup>th</sup> International Conference on Solid State Ionics, Halkidiki, Greece, 1999. Outstanding Poster Award.